THE ACOUSTIC SOURCE CREATED BY
TURBULENT FLOW
OVER ORIFICES AND LOUVERS

by

GLENN ERIC CANN and PATRICK LEEHEY

Report No. 97674
June, 1987

Acoustics and Vibration Laboratory

Massachusetts Institute of Technology
Cambridge, Massachusetts 02139

THE ACOUSTIC SOURCE CREATED BY TURBULENT FLOW OVER ORIFICES AND LOUVERS

by

Glenn Eric Cann and Patrick Leehey

Report No. 97674

June, 1987

Department of Mechanical Engineering

TABLE OF CONTENTS

LIST OF FIGURES

THE ACOUSTIC SOURCE CREATED BY TURBULENT FLOW OVER ORIFICES AND LOUVERS

by

Glenn Eric Cann
Patrick Leehey

ABSTRACT

Orifice and louver sound power spectra are investigated, using an intensity probe, at various wind speeds in a low noise, semi-anechoic, subsonic wind tunnel for free stream velocities below 50 meters per second. The radiated noise is created by turbulent flow over various orifice and louver geometries which are flushed mounted into the wall of a long duct. Five orifice samples of rectangular shape and various transverse dimensions as well as four louver samples with multiple rectangular and circular orifices are tested. Also investigated is the effect of the leading and trailing edge angle on the radiated sound power. The scaling laws of the excitation frequencies and the speed/power laws are presented for ratios of the boundary layer thickness to the transverse orifice dimension from 1.01 to 4.29. A detailed theoretical model is developed for rectangular shaped aperture orifices and louvers based on the work by Ffowcs Williams [9], Nelson [11], and Corcos [12]. The model describes the predominant variables which effect the radiated flow noise. To ascertain the validity of the model, it is used to collapse the experimental power spectra for two orifice and one louver geometry. The model showed excellent agreement with the actual sound power measurements. Directivity plots are also presented to further describe the orifice/louver source.

1. INTRODUCTION

1.1 Background

Turbulent flow over an orifice or louvered openings can generate high levels of broadband noise. This phenomenon has been known for some time [1] and early investigators like Dunham [2], Rossiter [3] and East [4] attempted to identify and control the high vibrational levels and possibly the radiated sound levels caused by the interaction of the flow over these openings. Recent work by Elder, Farabee and DeMetz [5] concentrated on the area of cavity resonance where the opening provides the feedback path between the closed acoustic cavity and the source, the turbulent flow. When the typical dimension of the cavity is large compared to the acoustic wavelength, the source can excite various room modes of the cavity. If the turbulent vortex shedding frequency coincides with one of these room modes, then a strong feedback will occur, resulting in an acoustic resonance of that mode.

If the cavity's volume is further increased, multiple room modes will be excited and the strong feedback mechanism will be lost. This results in a much broader acoustic response and at lower amplitude levels than the resonant case which is typically characterized by large amplitudes at very discrete tonal frequencies. In practice, the detection of resonating cavities is often easy due to their strong discrete tones. However, once these resonances have been corrected, or presumably prevented in the design, identifying the cause of the remaining flow noise becomes much more difficult. Possible contributors to the broadband flow noise are: (1) the turbulent boundary layer direct transfer of energy to the structure of the enclosed acoustic space, (2) the power flow through the opening (open window effect) caused by the acoustic field created by the upstream and downstream turbulent sources in the boundary layer, (3) the power flow into the acoustic space caused by the source created in the opening due to the driving aerodynamic field and the shear-layer edge interaction with the downstream edge of the orifice and (4) the vibrational excitation of the internal structure caused by the orifice source. The amount of noise which the latter contributes depends on the details of the internal structure and the orifice/louver attachment design. Therefore to predict the contribution from internal structure vibration, one must first determine the orifice source.

1

1.2 Content

The contribution of the first three possible contributors to the total power radiated into a closed acoustic space is analyzed based on the results from several experiments. It is shown that indeed the orifice source provides both the spectral character and the predominant amount of the total sound power. By analyzing and comparing the results with a derived equivalent source model, the nature of the source and the parameters which affect its strength and spectral character are identified. The analysis comes directly from experimental measurements taken in a subsonic wind tunnel at the M.I.T. Acoustic and Vibration Laboratory.

2. SOUND INTENSITY MEASUREMENTS

2.1 Why Measure Sound Intensity?

To describe an acoustic source, one must measure a quantity which is not dependent on the environment or the surroundings. The quantity most often identified to describe a source is its power. Knowing the source's power, its interaction in any known environment or any known surrounding can be determined.

Until recently, most all experimental measurements to describe an acoustic source were accomplished by measuring sound pressure. This quantity, however, was the result of a source's interaction with a specific environment and utilizing the experimental results in other applications was often difficult. One technique that was developed to overcome the difficulty in relating one environment to other was to isolate the source of interest and to simulate a free field environment in an anechoic chamber. Here the radiated sound pressure in air was measured, then related directly to the sound intensity. This technique has as its biggest limitation, the availability of an effective anechoic chamber, particularly for use in low frequency analysis at the low frequencies.

Another technique is to measure the intensity directly utilizing a sound intensity probe. The theory of intensity measurements comes directly from two fundamental properties of acoustics. Those are the conservation of momentum and the definition of intensity. Conservation on momentum states that:

$$\rho \partial v_r / \partial t = -\partial p / \partial r \qquad (2.1)$$

which can be solved for the radial component of the particle velocity, v_r

$$v_r = -(1/\rho) \int \partial p / \partial r \, dt \qquad (2.1a)$$

A finite difference approximation is used to calculate the pressure gradient using two identical microphones by

$$\partial p / \partial r = \lim_{\Delta r \to 0} (\Delta p / \Delta r) \approx (p_A - p_B) / \Delta r \qquad (2.2)$$

3

where A and B correspond to channels A and B for the respective microphone inputs and Δr is the finite microphone spacing. The instantaneous pressure is taken as the mean value of the two pressure signals,

$$p \approx (p_A + p_B)/2. \tag{2.2a}$$

The finite difference approximation is valid provided the separation distance, Δr, is small compared to the acoustic wavelength. Thus, a finite difference approximation error becomes significant at high frequencies. For a plane sinusoidal wave, propagating along the axis joining the two microphones, the finite difference approximation assumes the free field phase between the two microphone positions to be equal to $k\Delta r$, whereas the actual measured free field phase is $\sin(k\Delta r)$. Therefore, the measured intensity, I', is related to the actual intensity, I, by

$$I'/I = \sin(k\Delta r)/k\Delta r \tag{2.3}$$

and the resulting measured intensity underestimates the actual intensity by L_e at high frequency by

$$L_e = 10\log(\sin(k\Delta r)/k\Delta r). \tag{2.3a}$$

All the intensity measurements in this report were obtained with a spacing of $\Delta r = 50\ mm$. Thus the finite difference error for this spacing, at the upper analysis bandwidth frequency of $f = 1600\ Hz$, was $L_e = -1.7\ dB$.

From the definition of intensity and by substituting equations 2.2 and 2.2a, the measured sound intensity becomes

$$I_r = pv_r \approx -[(p_A + p_B)/2\rho\Delta r]\int(p_A - p_B)dt. \tag{2.3b}$$

By measuring the intensity over a control surface which surrounds the source, the power can be calculated from:

4

$$P = \int_A I_r \, dA \qquad (2.4)$$

The advantages of measuring intensity directly are: (1) the effects from diffuse noise contaminating the experimental results are eliminated since the integral of this noise intensity around any closed control surface is zero, (2) the sound power calculated describes the acoustic source in a form which is readily usable to design engineers, (3) measurements can be made in the source's near field and (4) there are no restrictions on the shape and size of the control surface. A simple yet effective analogy to describe the rationale in measuring sound intensity, thus power directly follows:

- In attempting to design a heating system, an engineer solicits specifications from two companies. One company describes its heating system by stating the electrical power and the thermal efficiency of the unit. The other company describes the temperature at various locations inside an experimental enclosure at steady state conditions.

It is obvious in this example that describing the temperature field within one environment is practically useless to the design engineer whereas knowing the power and thermal efficiency, the designer can determine the interaction of this source with his particular environment.

In the experiments which follow, every attempt was made to utilize the advantages of measuring intensity directly and simulating a free field environment by taking the measurements in a semi-anechoic chamber, thus minimizing any enclosure interactions which could affect the radiated sound power.

2.2 Ideal Versus Practical Sound Intensity Analyzer

2.2.1 Active and reactive sound fields

Sound fields exist in two parts: an active part which transports sound energy by virtue of the fact that the sound pressure and the particle velocity are in phase and a reactive part which stores sound energy and in which the sound pressure and particle velocity are in quadrature. A sound field is said to be more reactive the more energy is stored relative to that transported. Sound field reactivity is defined as the difference between the measured sound pressure level, L_p, and the maximum intensity level L_i.

5

2.2.2 Ideal sound intensity analyzer

An ideal sound intensity analyzer would measure only the active part of the total sound field and would indicate sound intensity values approaching $0 \; watts/m^2$ in a highly reactive (highly diffuse) sound field.

2.2.3 Practical sound intensity analyzer

A practical sound intensity analyzer can never display such a low intensity level due to the small but ever present phase-mismatch between the two microphone channels. It is this phase mismatch which accounts for the lower limit in the dynamic range of a practical sound intensity analyzer.

2.3 Determining the Limits of Error for the Measured Intensity

Errors are introduced in any practical intensity measurement by:

1. the influence of the phase mis-match in the probe, ϕ_m and the analyzer, ϕ_a,

2. the influence of the phase of the sound field of known reactivity, ϕ_f, and

3. using a particular spacer between the two microphones.

The limits of these errors can be determined using a phase-reactivity nomogram [see reference 6]. This nomogram graphically determines, ϕ_f for a given measured reactivity $(L_i - L_p)$ and a particular spacer, Δr, according to the relationship:

$$L_i - (L_p + 0.16) = 10 \; \log[1000/\Delta r \times C/f \times \phi_f/360] \qquad (2.5)$$

The phase of the sound field, ϕ_f, together with the phase of the probe and the analyzer, $\phi_f - \phi_a - \phi_m$ and $\phi_f + \phi_a + \phi_m$, set the limits of error in the measured phase at a particular frequency. From these phase limits, the nomogram provides the limits of error in dB for the measured intensity.

6

2.4 Sound Intensity Probe

The specific details on the operation of the intensity probe used in this experiment are contained in reference (7). Briefly, the intensity probe consists to two B & K phase matched, 1/2" condenser microphones, type 4177/4165, separated by a spacer 50 mm in length and on a common axis. One microphone is a reference while the other microphone provides the pressure gradient measurement.

2.5 Intensity Measurements

2.5.1 Calculating intensity

Sound intensity measurements were analyzed using a B & K 2032 Spectrum Analyzer. The sound intensity was calculated according to the relationship:

$$I(k) = -(1/\omega \Delta r_\rho) Im\overline{[G_{AB}(k)]} \tag{2.6}$$

where Δr is the microphone spacing in meters, A corresponds to Channel A which is the reference microphone input, B corresponds to Channel B which is the second microphone input, k is the frequency index and ρ is the density of air, calculated according to the relationship:

$$\rho = 0.348534p/(273 + T) \tag{2.7}$$

where p is the pressure in mbar and T is the temperature in degrees centigrade.

The cross spectrum, $G_{AB}(k)$, is the complex ensemble average of the complex products of the complex conjugated one-sided instantaneous spectrum $G_A(k)$ and the one-sided instantaneous spectrum $G_B(k)$.

$$\overline{G_{AB}(k)} = \overline{G_A(k) \cdot G_B(k)} \tag{2.8}$$

The instantaneous one-sided spectrum for channel A or B, $G_A(k)$, $G_B(k)$ was calculated according to:

$$G_A(k) = \begin{cases} S_A(k) & \text{for } k = 0 \\ 2S_A(k) & \text{for } 1 < k < N/2 - 1 \\ 0 & \text{for } N/2 < k < N - 1 \end{cases} \qquad (2.9)$$

where N is the number of samples per ensemble. For this experiment, N was equal to 1024. $S_A(k)$ is the two-sided instantaneous spectrum for channel A which is determined from the recorded time record, a(n) according to:

$$S_a(k) = \mathcal{F}[\omega(n) \cdot a(n)] \qquad (2.10)$$

where $\mathcal{F}$ is the forward discrete fourier transform and $\omega(n)$ is the time record weighting function. In this experiment, a Hanning window weighting function was utilized.

The forward discrete fourier transform, $\mathcal{F}$, is defined as:

$$S_A(k) = 1/N \sum_{n=0}^{N-1} a(n) \cdot exp(-j2\pi kn/N) \qquad (2.11)$$

where n equals the time index times the sampling interval, $n\Delta t$ and k equals the frequency index times the frequency resolution, $k\Delta f$. The frequency resolution for this experiment was 2 Hz for an analysis bandwidth of 1600 Hz.

2.5.2 Measurement techniques

Two techniques can be used to measure sound intensity using an intensity probe. They are:

1. continuous spatial averaging

2. discrete point averaging

Continuous spatial averaging consists of sweeping the intensity probe at a controlled rate over each surface while continuously sampling and averaging data. This technique produces the most accurate spatially averaged results but suffers slightly in repeatability. Several repeated runs, often four or more, were required to obtain the required repeatability of total sound power (within 0.5

8
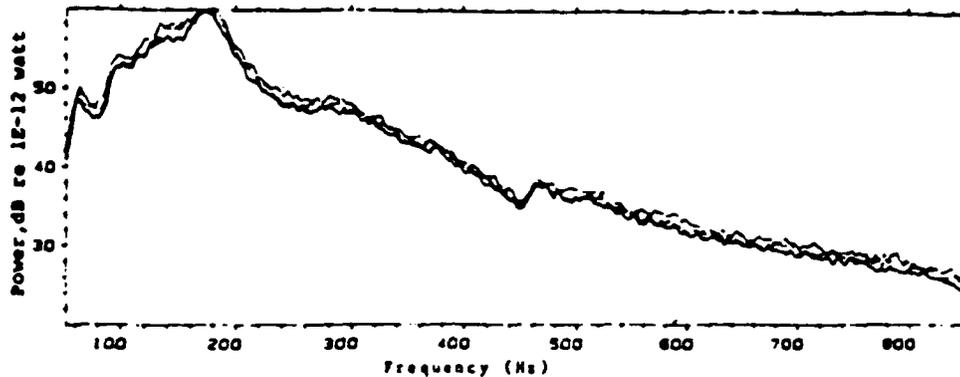
Figure 1: Louver L1 sound power spectra repeatability. Shown are four successive spectral measurements of sound power.

dB on at least three runs). Figures 1, 2 and 3 are the results of three such repeatability experiments with 0.5 dB or less variation in total sound power. Shown is the sound power spectral level from a rectangular orifice, $4 - 1/2''$ by $1 - 2/3''$, and an analysis bandwidth of 2 Hz.

Discrete point averaging consists of dividing your control surface into numerous discrete areas and measuring the sound intensity at the center of each discrete area (point) and summing over all areas. This technique offers maximum repeatability but at reduced spatially-averaged accuracy. The two techniques were both utilized initially and compared. The repeatability of the total radiated power using the discrete point technique, with 45 points, was 0.3 - 0.5 dB between successive runs. These repeatability values were selected as the criteria for the continuous spatial averaging technique. The results showed that the two techniques gave similar sound power spectrums and similar total sound power levels within an accuracy of 0.3 dB. For this reason, the continuous spatial averaging technique was selected due to its increased accuracy and reduced sampling time.

The control surface was constructed of $1/4''$ balsa wood enclosing a total

9
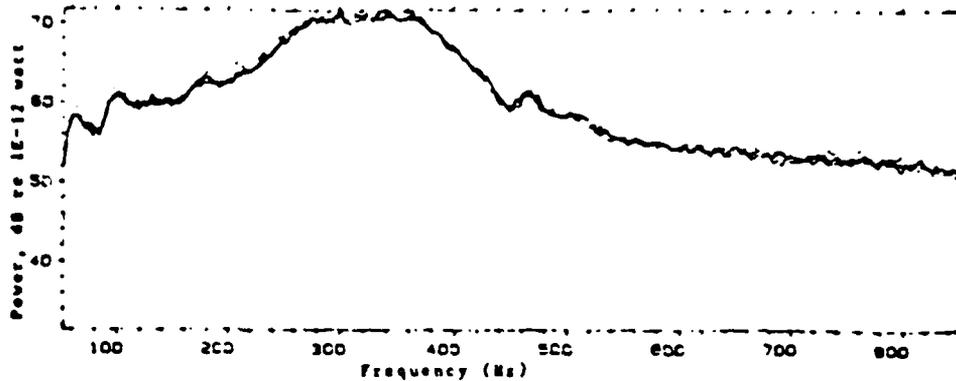
Figure 2: Orifice O1 sound power spectra repeatability. Shown are three successive spectral measurements of sound power.
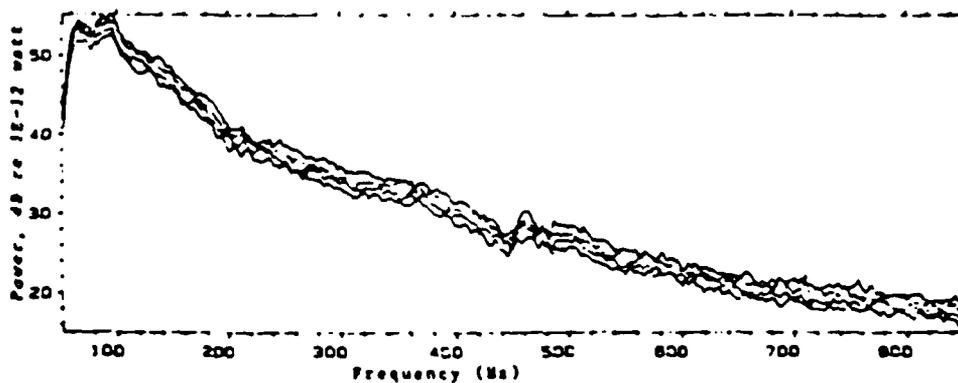
Figure 3: Orifice O1 sound power spectra repeatability. Shown are five successive spectral measurements of sound power.

10
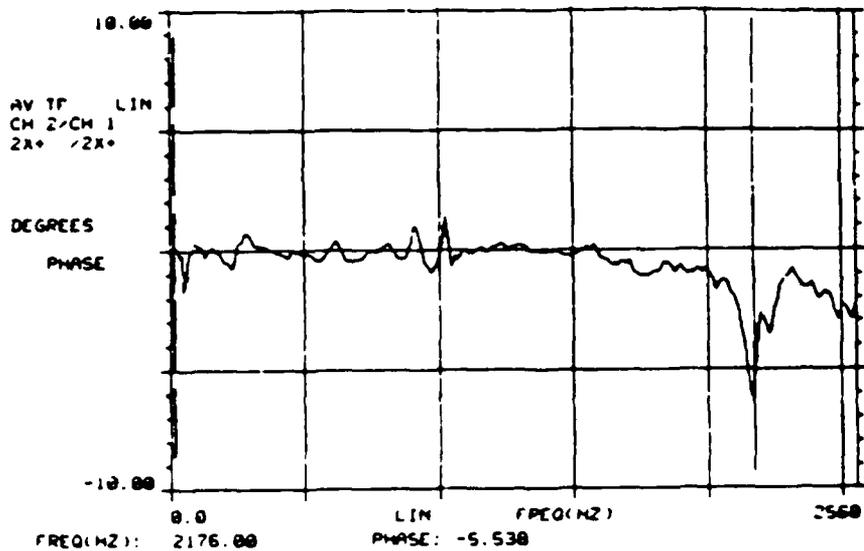
Figure 4: Phase difference between two microphones and their preamplifiers (channels A and B)

surface area of 0.542 square meters. Intensity spectra over the frequency range of 52-1600 Hz were taken and recorded on a B & K 2032 Spectrum Analyzer. Microphone calibration was performed using a pistonphone and daily temperature and barometer measurements were taken to calculate the air density. To ensure that the two microphone were indeed phase matched, their phase was measured in a random noise field and compared. The microphones were placed at the open end of a long cylinder, equal distances from a speaker placed at the opposite end of the cylinder. This apparatus was similar in design to a calibration pistonphone, type 4200. Figure 4 shows the phase difference measured over a frequency range of 2560 Hz and clearly demonstrates their compatibility over the frequency band of interest, 52 - 1600 Hz.

11

In Section 5.2, the errors in dB resulting from these phase mismatches are calculated and shown to be on the same order of magnitude as the inherent statistical fluctuations.

2.5.3 Power spectrum contamination

Data below 52 Hz were ignored due to contamination by the 1,0,0 room mode (38 Hz) of the semi-anechoic chamber. Also at this low frequency, the effectiveness of the anechoic treatment was reduced. The peak at 462 Hz and its harmonic at 924 Hz which is evident in all the spectra was due to the resonance of the cross-duct mode of the test section and not at all associated with the orifice source. Fortunately, the sound level and narrow bandwidth associated with this modal resonance contributes insignificantly to the total sound power caused by the orifice source. Frequencies above 1600 Hz contributed nothing to the total sound power and the spectral shape followed the same trend as from 1200 - 1600 Hz.

3. THEORY

3.1 Introduction

The development of a theoretical model to determine the scaling laws for orifice/louver flow noise was first accomplished in 1972 by Ffowcs Williams [8]. He treated the model problem of flow noise generated by a body of turbulence near an infinite, rigid, thin screen with circular orifices. His assumptions were: a) the size of the orifice is much smaller than the distance between them, b) variations in pressure within individual apertures are neglected. While these assumptions are rather restrictive in their application to many industrial louvers, the theory does provide a fundamental result: that the sound radiated by orifices and louvers can be directly related to the mass flow driven through the aperture by the aerodynamic field.

This fundamental result was used by Nelson [9] to develop a model for flow noise generated over practical perforated screens with circular orifices. Due to the normal component of the turbulent fluctuations above the louver, flow is driven through the orifice resulting in a fluctuating volume flow through the upper surface. This fluctuating volume flow constitutes an equivalent monopole source at the upper surface. Since the volume flow into the upper surface of the orifice creates an equivalent outflow through the lower surface, there is an equal and opposite equivalent monopole at the lower surface. The net field which radiates out of the louver and into the closed acoustic space is thus the combination of the lower monopole source and the contribution from the upper monopole source which is dependent on the degree of acoustical transparency of the louver. If the louver is acoustically opaque, then only the lower monopole source will radiate into the acoustic space. If the louver is acoustically transparent, then the upper monopole source will radiate into the space, having a cancelling effect on the field of the lower monopole source. This would result in a net radiated field which exhibits properties of a dipole source.

Nelson's equivalent source model gave an excellent description of the flow noise produced by perforated facing materials used in practice even though he assumed a rather simplistic form for the driving aerodynamic velocity. His assumptions were: a) the wavelength for the sound is much larger than the orifice radius, b) there are many apertures per acoustic wavelength and no interactions of the flow occurred between adjacent apertures which can modify the aperture's conductivity. In the sections that follow, the theory developed by Nelson and Ffowcs Williams will be utilized to model the flow noise created by turbulent flow

13
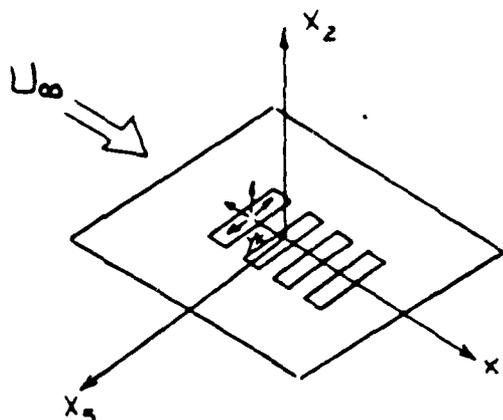
Figure 5: Coordinate system for analysis

over orifices and louvers. Once the equivalent source model has been developed, it will be used to collapse the experimental sound power spectra thus providing a verification to the theory's validity. The coordinated system used for this analysis is shown in Figure 5.

3.2 The Equivalent Source Model for Orifices and Louvers

Ffowcs Williams [8] and Leppington and Levine [10] developed an expression for the reflection coefficient, R, for a plane wave of single frequency, ω, incident at a polar angle, θ, on an infinite louver. For low frequencies and orifice spacings that are large compared to the orifice size, the reflection coefficient, R, is

$$R = 1/(1 + 4\, ai N/k \cos\theta) \qquad (3.1)$$

where a is the orifice radius, N the number of orifices per unit area of louver and k is the acoustic wavenumber, $k = \omega/Co$.

The field produced by the lower monopole at y_k can be determined using the principle of reciprocity. The field at y_k due to a distant source at x_k, is given by

14
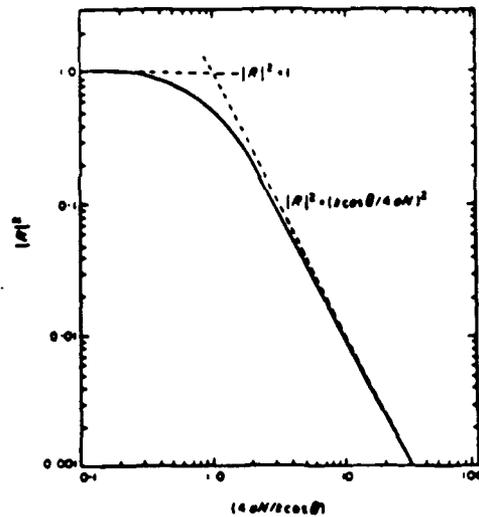
Figure 6: The infinite screen reflection coefficient as a function of the ratio $(4aN/k\cos\theta)$. From [9, Nelson, P.A., 1982].

$p_i(1 + R)$ where p_i is the incident plane wave striking the lower surface of the louver. Thus one can write

$$P(y_k) = (1 + R)Q(x_k)exp(ik \mid y_k - x_k \mid)/4\pi \mid y_k - x_k \mid \qquad (3.2)$$

where Q is the strength of the distance monopole at x_k. By reciprocity, the field at x_k due to the monopole at y_k is given by interchanging the source and receiver position vector in equation 3.2. Equation 3.2 can be generalized to relate the spectral density of the acoustic pressure field, $S_p(x_k, \omega)$ to the spectral density of the source $S_Q(y_k, \omega)$ such that

$$S_p(x_k, \omega) = \mid 1 + R \mid^2 \cdot S_Q(Y_k, \omega)/16\pi^2 r^2 \qquad (3.3)$$

where $r^2 = \mid x_k - y_k \mid^2$. Figure 6 is a plot of $\mid R \mid^2$ against the ratio $(4aN/k\cos\theta)$.

From this plot, it can be seen that,

$$\mid R \mid^2 = 1 \quad \text{for} \quad (4\,aN/k\cos\theta) \leq 0.3$$

15

This occurs for open area ratios on the order of 0.01 (see reference 11). For all the orifice and louvers tested in this study, the open area ratio is less than 0.005 so that $|R|^2 = 1$. To verify this result for the reflection coefficient, since the assumption of many apertures per acoustic wavelength is not valid for the single orifice, a separate analysis was performed. Here, in two dimensions, the plane wave of single frequency, ω, is incident normal on an infinite, rigid surface with a single opening, of dimension, 2b. Again the principle of reciprocity is used to predict the radiated pressure from the single orifice. Using matched asymptotic expansions, for $b/\lambda \ll 1$, the lowest order solution for the reflection coefficient is again, $|R|^2 = 1$. The details of this analysis are shown in Appendix 1.

Thus,

$$S_p(x_k, \omega) = S_Q(y_k, \omega)/4\pi^2 r^2 \tag{3.4}$$

The instantaneous source strength $q(y_k, t)$ can be written in terms of the weighted integral of the unsteady normal component of velocity over the area of the aperture. To take advantage of the homogeneous and stationary properties of the velocity in the plane of the wall, we can write

$$q(y_k, t) = -i\omega p \int_\infty \int_\infty v(y_k, t) K(s_k - y_k) dA(s_k) \tag{3.5}$$

where y_k is the vector position of some reference point on the aperture surface and $K(s_k - y_k)$ is the weighting function, i.e., the function which converts the integral over the aperture area, $s_k = s_1, s_2$, to an integral over all space, defined as

$$K(s_k - y_k) = 1 \quad \text{for} \quad s_k - y_k \quad \text{inside of the aperture area,} \quad A$$
$$= 0 \quad \text{for} \quad s_k - y_k \quad \text{outside} \quad A$$

Following Corcos [12] the spectral density of the source strength, $S_Q(y_k, \omega)$ can be defined by

$$S_Q(y_k, \omega) = \rho^2 \omega^2 \int_\infty \int_\infty S_{vv}(z_k - s_k, \omega) K(z_k) K(s_k) dA(z_k) dA(s_k) \tag{3.6}$$

16

where z_k is a dummy space vector. Define ϵ_k by

$$\epsilon_k = z_k - s_k$$

thus

$$S_Q(y_k,\omega) = \rho^2\omega^2 \int_\infty \int_\infty S_{vv}(\epsilon_k,\omega) K(s_k) K(s_k + \epsilon_k) dA(s_k) dA(\epsilon_k)$$

$$= \rho^2\omega^2 \int_\infty S_{vv}(\epsilon_k,\omega)\theta(\epsilon_k)dA(\epsilon_k) \tag{3.6b}$$

where the function, $\theta(\epsilon_k)$, defined as the orifice response function, is determined wholly by the geometry of the aperture and can be evaluated as

$$
\begin{aligned}
\theta(\epsilon_k) &= \int_{-\infty}^\infty K(s_k + \epsilon_k)dA(s_k) = 1 \times \text{area of overlap} \\
&= (L- \mid \epsilon_3 \mid)(b- \mid \epsilon_1 \mid) \quad \text{for} \quad \mid \epsilon_3 \mid \le L, \mid \epsilon_1 \mid \le b \\
&= 0 \quad \text{elsewhere}
\end{aligned}
\tag{3.6c}
$$

for the rectangular shaped orifice shown below
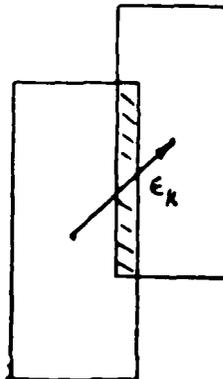
Finally, we assume the cross-spectral density, $S_{vv}(\epsilon_k,\omega)$, to have the product

17

form

$$S_{vv}(\epsilon_k, \omega) = S_v(\omega) A(K\epsilon_1) B(K\epsilon_3) e^{iK\epsilon_1} \tag{3.7}$$

where $S_v(\omega)$ is the spectral density of the normal velocity fluctuations, K is the convective wavenumber given by $K = \omega/U_c$ where U_c is the convection speed of the boundary layer eddies and $A(K\epsilon_1)$ and $B(K\epsilon_3)$ are the amplitude functions for the normalized longitudinal and lateral cross-spectra, respectively. This form is similar to the expression given by Corcos [12] for the cross spectral density of the boundary layer pressure fluctuations. The longitudinal cross-spectra of the eddies as they convect in the y_1 direction also contains the phase term $exp(iK\epsilon_1)$. $A(K\epsilon_1)$ is plotted in Figure 7 as a function of its argument for various ratios of separation distance to momentum thickness (r_1/δ^*) for wall pressure. Since the wall pressure is related to the volume integral of the normal component of the velocity, wall pressure cross-spectra data can be used to predict the longitudinal and the lateral cross-spectra of the normal component of particle velocity. Comparing the wall pressure correlation length scales from [12] to the velocity correlation length scales from [17], we find that both the longitudinal and lateral length scales agree to within an order of magnitude, thus supporting the previous statement.

For the various orifice and louver samples tested, at a maximum value for r_1/δ^* equal to 1, $A(K\epsilon_1)$ varies from a maximum value of 1 to a minimum value of 0.6 for orifice 02 at $U = 20m/s$ and $f = 250$ Hz (the frequency at which the spectral level is 10dB down from the peak level). Throughout most of the samples tested, $A(K\epsilon_1) = 1$ over the frequency band of interest. Thus the longitudinal correlation lengths were typically several times the length of the orifice aperture. Thus the assumption is made that no decay in the eddy structure occurs in the longitudinal (y_1) direction.

The normalized lateral cross-spectra in the y_3 direction is given by the term $B(K\epsilon_3)$ which is assumed unity for no separation and to decay very rapidly with increased separation. To justify this assumption, $B(K\epsilon_3)$ is plotted in Figure 8 as a function of its argument for various ratios of r_3/δ^*. From this figure, the typical correlation length, ℓ, is calculated to be on the order of 2 cm. The ratio of the lateral correlation length, ℓ, to the aperture length, L, is 0.18 thus supporting the initial assumption of rapid lateral decay. The correlation lengths are determined at the point where the amplitude function equals 0.4 and at the frequency corresponding to the peak power spectral level.

18
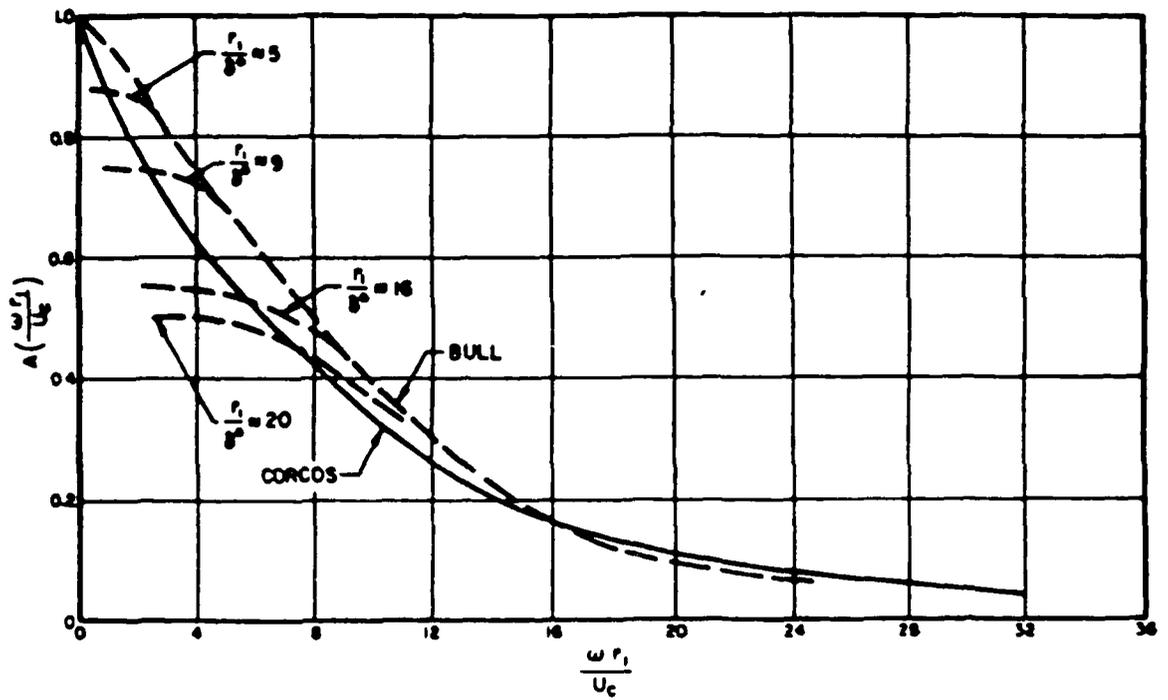
Figure 7: Amplitude function for longitudinal cross-spectral density of wall pressure. From [16, BBN report No. 4110366, 1966]

19
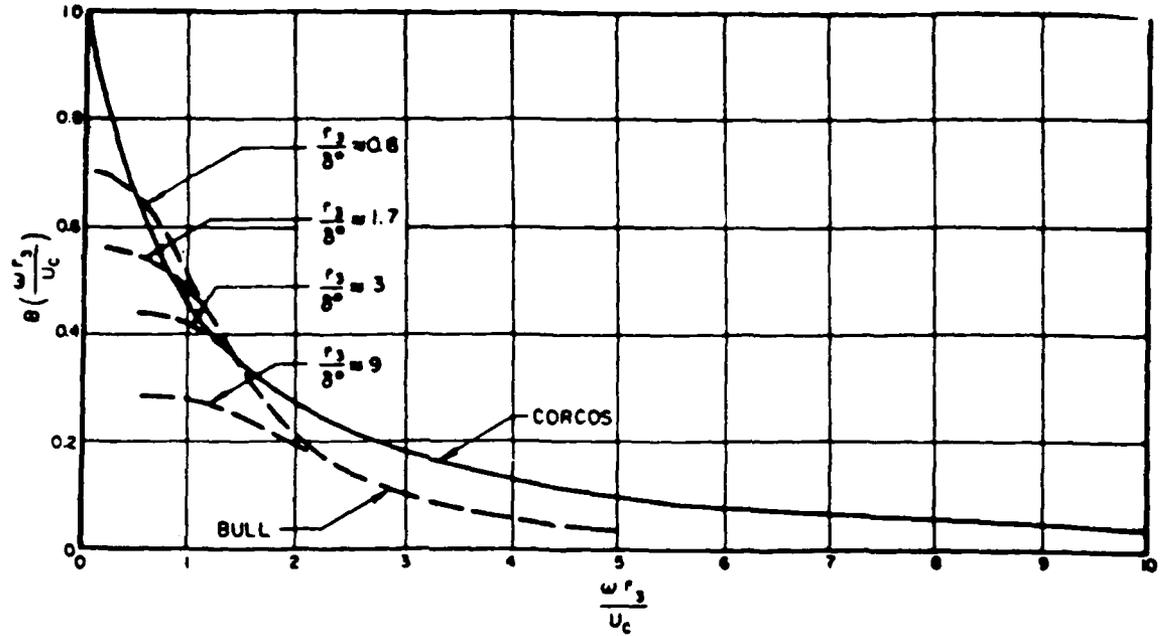
Figure 8: Amplitude function for lateral cross-spectral density of wall pressure.
From [16, BBN Report No. 4110366, 1966]

Substituting equation 3.7 into equation 3.6b and evaluating the integral over the rectangular shaped orifice, assuming $S_v(y_k,\omega)$ to be uniform over the orifice area gives:

$$S_Q(y_k,\omega) = p^2\omega \cdot S_v(y_k,\omega) \cdot L\ell \cdot (2/K^2)(1 - cos(Kb)) \qquad (3.8)$$

where L is the orifice length in the y_3 direction. See Appendix (3) for the details of the integration for the rectangular shaped orifices and reference [9] for the results for circular shaped orifices. Equation 3.8 states that the monopole spectral density is directly related to the normal velocity spectral density.

3.3 Scaling Laws for the Radiated Sound Power

Having determined the form for the source strength, we can now develop the scaling laws for the radiated sound power from various rectangular shaped configurations. Assuming that each orifice radiates sound incoherently, the total source strength for N apertures is simply N times the individual source strength for each aperture defined by equation 3.8. Substituting equation 3.8 into equation 3.4 gives:

$$S_p(x_k,\omega) = N\rho^2 L\ell \cdot S_v(y_k,\omega)(1 - cos(Kb))U_c^2/2\pi^2 r^2 \qquad (3.9)$$

The assumption is made that the convection velocity, U_c, is equal to one half the freestream velocity, U_∞. Define the turbulent intensity, I, and the Strouhal number, $St(\ell)$ and $St(b)$ by:

$$(I^2)_{\Delta\omega} = 1/U_\infty^2 \cdot \int S_v(y_k,\omega)d\omega \qquad (3.10)$$

$$St(\ell) = f\ell/U_\infty, St(b) = fb/U_\infty \qquad (3.11)$$

Finally, integrating equation 3.9 over the bandwidth $\Delta\omega$ with the above expressions substituted, yields

21

$$\overline{p^2(x_k,t))}_{\Delta\omega} = N\rho^2 L \cdot (1 - cos(Kb))St(\ell)(I^2)_{\Delta\omega}U_\infty^5/2f\pi r^2 \qquad (3.12)$$

For spherical waves, the sound power, P, can be determined by:

$$\overline{(P(t))}_{\Delta\omega} = N\rho L(1 - cos(Kb))St(\ell)(I^2)_{\Delta\omega}U_\infty^5/fCo \qquad (3.13)$$

Equation 3.13 is the final result for the flow noise created by turbulent flow over orifices and louvers with rectangular shape as described in Section (4.2). The controlling parameters for scaling sound power are thus:

1. Strouhal number based on the lateral correlation length, ℓ and aperture transverse dimension, b

2. the normal component of the Turbulent Intensity

3. the fifth power of the freestream velocity

4. the shape factor $(1 - cos(Kb))$

In Section (5.10), this model is used to collapse the experimental sound power data for orifices 02 and 03 and louver $L1$. It is clear from the collapse that equation 3.13 does indeed identify the predominant controlling parameters for rectangular shaped orifice and louver flow noise. Note, for circular shaped apertures, the above scaling factors remain the same except the shape factor is replaced by the function, $H_1(Kd)$ where H_1 is a Struve function of the first kind and d is the aperture diameter. See reference 9 for the details in calculating equation 3.8 for a circular aperture.

22

4. EXPERIMENTAL APPARATUS

4.1 Semi-anechoic Wind Tunnel

The experiments were carried out using the low turbulence, sub sonic wind tunnel of the Acoustics and Vibration Laboratory at MIT. The wind tunnel details are shown in Figure 9 with the basic construction characteristics described by Hanson [13] and modifications described by Shapiro [14]. The wind tunnel is of open circuit design with the test section enclosed in a blockhouse. The tunnel consists of a set of flow straighteners, screens, a settling chamber and a 20:1 contraction leading to a square test section 38cm by 38cm. The blockhouse walls, floor and ceiling were treated with urethane foam to provide a semi-anechoic chamber within which acoustic intensity measurements were taken. Figure 10 details a cut-away front and top view of the chamber and test section. The acoustic treatment consisted of a base of 10cm foam, then a set of 10cm foam cubes spread randomly and finally a set of 2cm ɔam cubes also spread randomly. The effectiveness of the coating was determined by [14] using a horn driver and measuring the sound field decay with distance. The anechoic treatment was effective between 200 Hz and 2000 Hz and only partially effective at 100 Hz.

4.2 Orifice/Louver Samples

Nine separate orifice/louver samples were tested. All samples were made of plexiglass and screwed into the sample mounting window which was mounted flush into the side to the test section as shown in Figure 10. The separate samples tested were:

1. O-1: a $4 - 1/2''$ (height) by $1 - 2/3''$ (width) rectangular orifice, $3/4''$ thick with straight sided walls

2. O-2: the above made of $1/4''$ thick plexiglass

3. O-3: a $4 - 7/16''$ by $27/64''$ rectangular orifice, $1/4''$ thick with straight sided walls

4. O-2A: O-2 with 40 degree slanted walls, i.e, both walls form an angle of 40 degrees towards upstream from the perpendicular to the flow.

5. O-3A: O-3 with 40 degree slanted walls

23
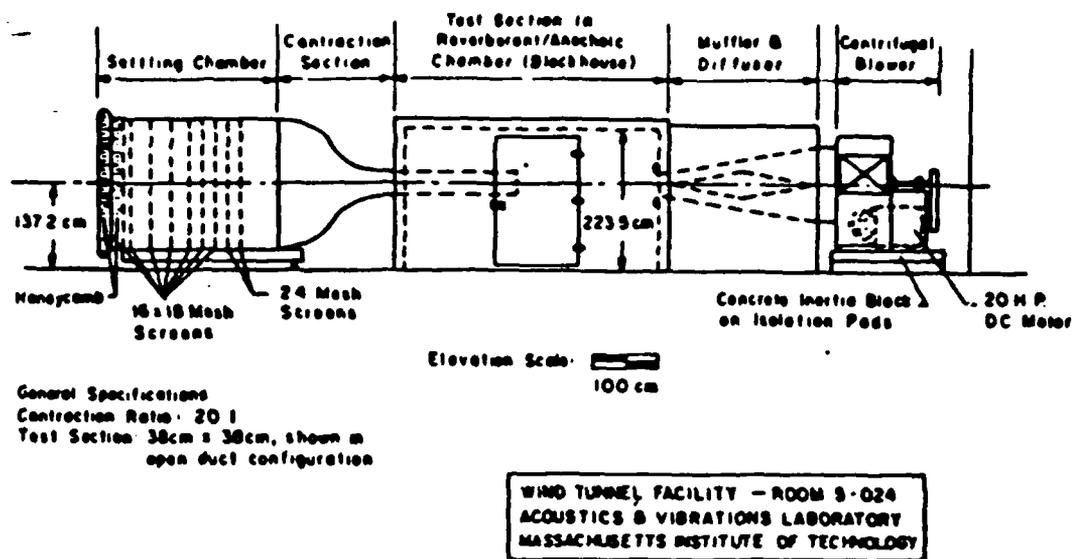
Figure 9: Wind Tunnel Facility

6. L-1: 4 rectangular orifices, each $4-7/16''$ by $27/64''$, separated by $1/4''$, $1/4''$ thick

7. L-2: 54 circular orifices, each $27/64''$ in diameter, separated by $0.6328''$ between centers, $1/4''$ thick

8. L-1A: L-1 with 40 degree slanted walls

9. L-2A: L-2 with 40 degree slanted walls.

The louver configurations were designed to maintain the same total open area as the single orifices, O-1 and O-2. The 40 degree slanted walls provided a blunt orifice trailing edge and subsequently a sharp orifice leading edge, as seen from the flow.

4.3 Test Section

The test section was made from $3/4''$ finished plywood, 38 cm by 38 cm square in cross section and was located on the centerline of the chamber. The test section was sealed and the ends were further covered by $2''$ of urethane foam.

24

FRONT VIEW

Labels in figure: Sound Isolation Mounts; Louver (¼" plexiglass); Sample Mounting Window; 4" Foam

TOP VIEW

Labels in figure: Semi-anechoic foam blocks; 4" foam; Louver; Control Surface; Intensity Probe
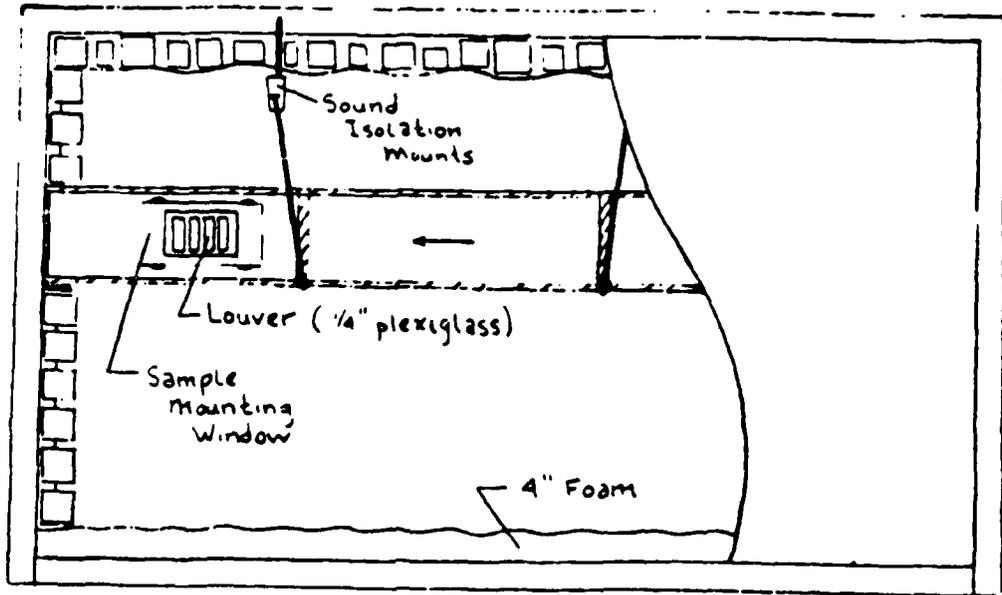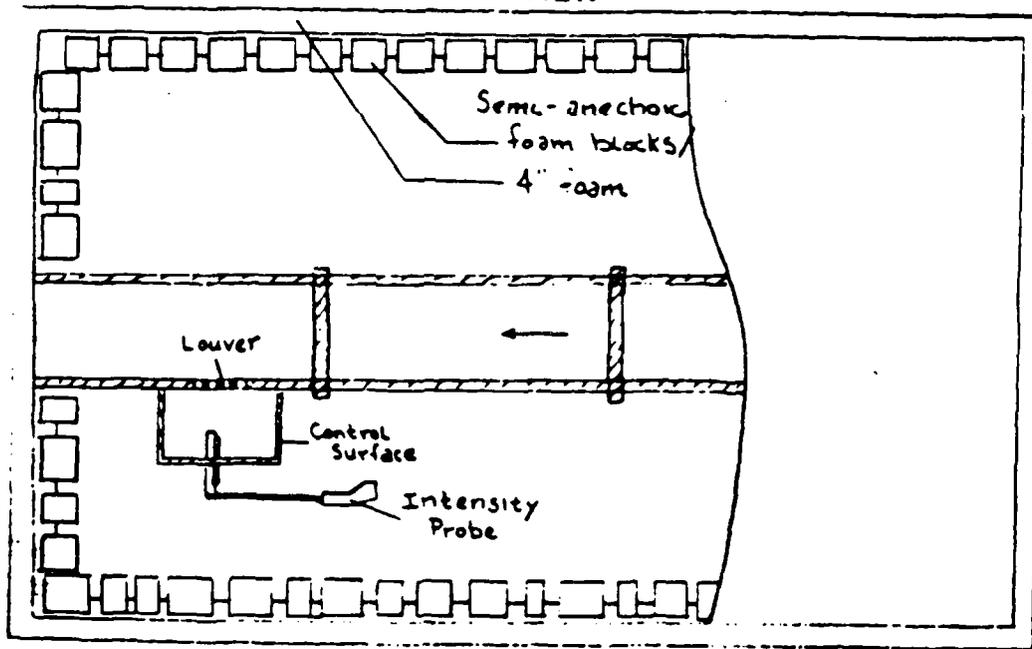
Figure 10: Experimental set-up within the wind tunnel, front and top views

The background power levels, measured with the orifice covered, were sufficiently low compared to the power levels with the orifice exposed (see Section 5.3) to ensure signal to noise ratios of at least 10 dB over the frequency range of interest and at all operating speeds.

4.4 Turbulent Intensity Measurements

Turbulent Intensity is defined by the relationship:

$$TI = 20\log(\sqrt{u^2}/U_\infty \tag{4.1}$$

Turbulent fluctuations were measured using a Dantec Constant Temperature Anemometer with a 5 micron diameter tungsten wire. The output of the anemometer, being the total voltage E, was inputted directly to the B & K 2032 Spectrum Analyzer. Here the AC-coupled autospectrum, $G_E(\omega)$, was measured. The mean-squared fluctuating velocity autospectrum, $G_u(\omega)$ was determined from:

$$G_u(\omega) = (\mid H \mid^2)G_E(\omega) \tag{4.2}$$

where H is the transfer function. See Appendix 2 for the details in determining H. Turbulent Intensity spectra were measured at all four flow speeds for orifice 0-2 and louvers $L-1$ and $L-1A$. The position of the U probe was:

1. two-tenths of an inch into the boundary layer directly above the orifice at both the upstream and downstream edge. For the louvers, the streamwise measurements were taken in the center of the furthermost upstream and downstream orifice,

   and

2. half-way into the throat of the orifice and at the same streamwise locations as described above.

5. EXPERIMENTAL RESULTS

5.1 Introduction

Figure 11 shows the geometry of the problem. Air flows at free speed U_∞ over an orifice or louver which has been inserted flush into a long flat walled duct. The orifice was either rectangular, with streamwise dimension b and length L or circular with diameter d. The acoustic radiated power from the orifice/louver was measured at free stream velocities of 20, 30, 40 and 50 meters per second. The acoustic power was determined by sweeping the intensity probe over a control surface (a five sided boxed frame surrounding the orifice) then multiplying the resulting spatially and temporally averaged intensity by the total surface area of the control surface. Five orifices and four louvers were tested as described in Section 4.2.

To determine the contribution made solely by the orifice/louver source, two additional experiments were conducted. One experiment consisted of measuring the acoustic power radiated by the duct when the orifice was covered. The second experiment consisted of measuring the power flow through the orifice, in the absence of free stream flow, due to an artificially created acoustic field in the duct. This field was created using a speaker in the duct and was equal in magnitude to that caused by the turbulent boundary layer at $U = 50\ m/s$. This experiment determined the "open-window" contribution to the overall sound power. Finally, directivity measurements were taken for orifice 0-2 and louver $L - 2A$ at $U = 25\ m/s$ and the respective polar plots produced.

5.2 Reactivity of the Sound Field and Sound Intensity Error Limits

The reactivity of the sound field in the blockhouse (the closed acoustic space) was measured for various orifice and louver samples (see Figures 12 and 13). The Table below lists the measured difference between the total sound pressure level, L_p and the total sound intensity level, L_i, for the orifice O2A and the louver $L2A$ at a radial distance of 2 feet.

Sample	Reactivity $(L_p - L_i)$	$U_\infty\,(m/s)$
O2A	0.8	30
	1.0	50
L2A	0.9	30
	1.0	50

Table 1: Measured Sound Field Reactivity

27
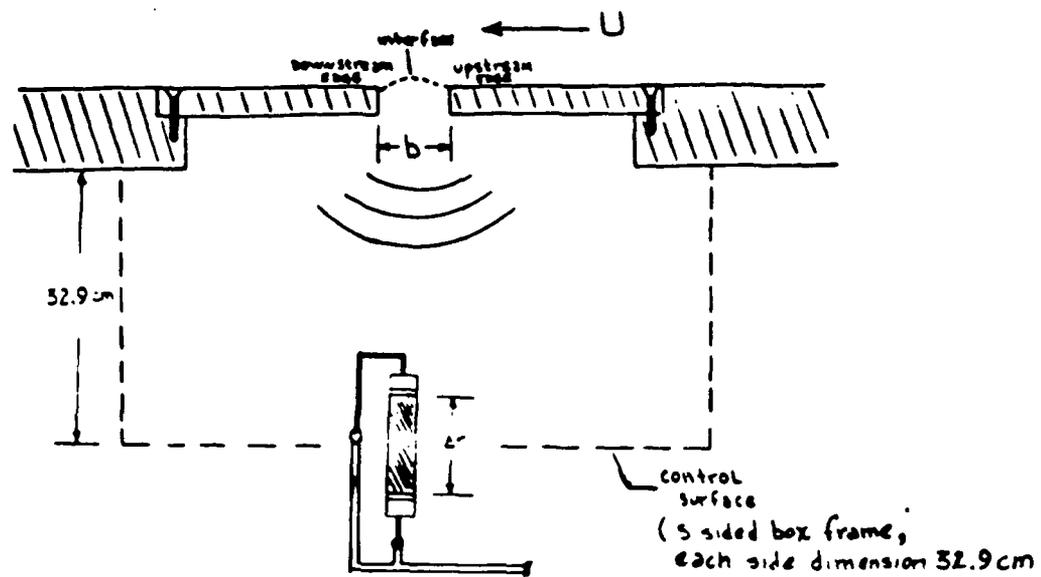
Figure 11: Schematic of orifice and probe geometry. Air flows at freestream velocity, U, over an aperture of streamwise dimension, b. Sound intensity is measured by probe (microphone spacing, Δr) while continuously sweeping control surface.
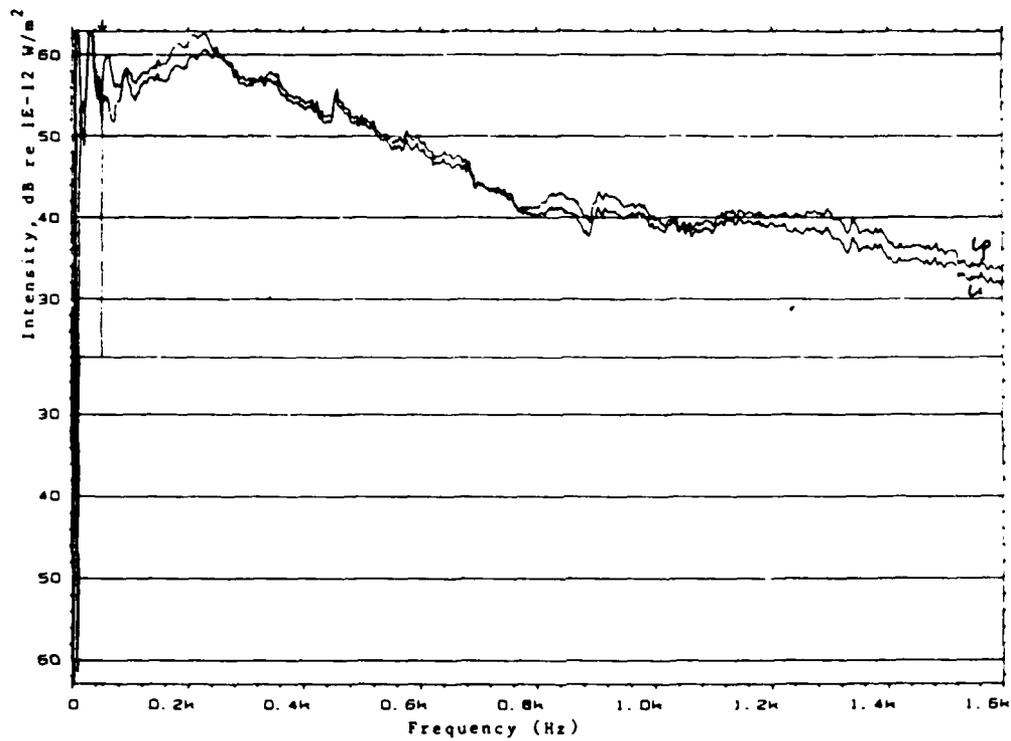
Figure 12: Sound field reactivity for orifice O2A. Shown are the sound intensity and sound pressure spectral levels. The difference between the two is defined as the sound field reactivity.
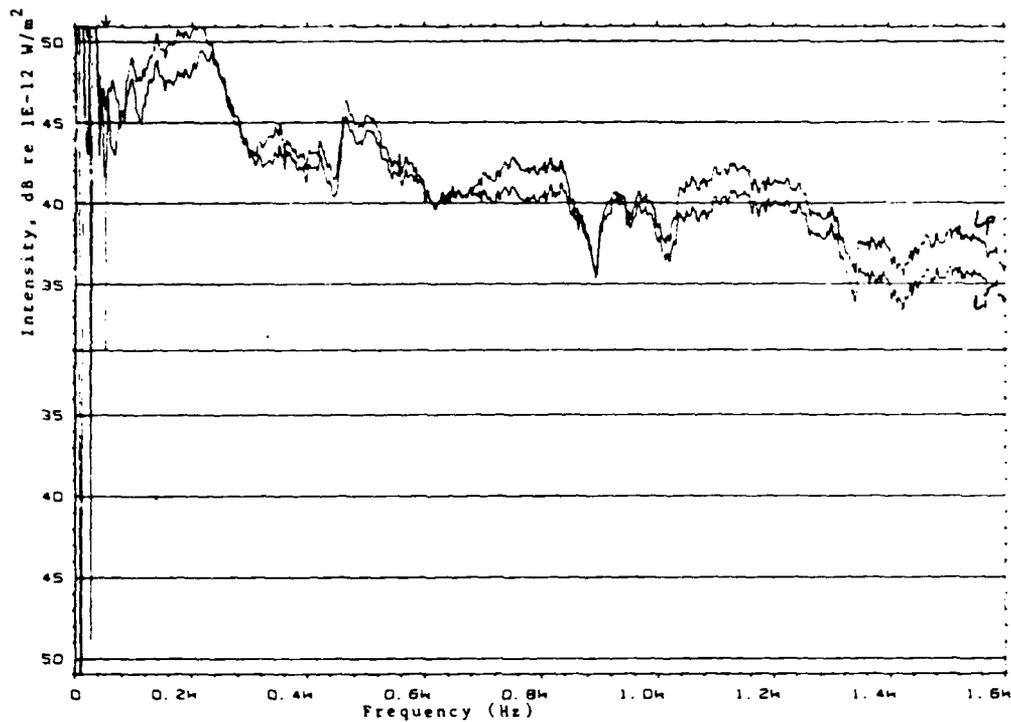
Figure 13: Louver *L2A* sound intensity spectral levels versus sound pressure spectral levels ($L_i vs. L_p$). The difference between L_i and Lp is defined as the sound field reactivity.

30

From Figure 4, the measured phase-mismatch for the sound intensity probe is:

Frequency (Hz)	$\phi_m(degrees)$
63	0.8
500	0.2
1000	0.5
2000	0.9

The maximum phase-mismatch between channels A and B for the Analyzer is 0.3 degrees. With a spacer value of $50mm$ and the above sound field reactivity, the phase reactivity nomogram of reference 6 gives the following value for the maximum phase of the sound field, between the two microphone positions.

Frequency (Hz)	$\phi_m(degrees)$
63	2
500	16
1000	25
2000	60

Therefore the limits of the phase-mismatch are:

| Frequency(Hz)	$\phi_f - \phi_a - \phi_m$ (degrees)	$\phi_f + \phi_a + \phi_m$ (degrees)
63	0.9	3.1
500	15.5	16.5
1000	24.2	25.8
2000	58.8	61.2

The above total phase-mismatch values are the limits of error in the measured phase at the frequency listed. The corresponding limits in dB for the measured intensity from the nomogram are:

Frequency (Hz)	Error limits (dB)
63	+ 2.5
500	+ 0.5
1000	+ 0.25
2000	+ 0.125

31

The corresponding statistical standard deviation, ϵ, of the measured spectral levels about the mean value is:

$$\epsilon = 4.34/\sqrt{BT_a}, (dB) \tag{5.1}$$

where B is the filter bandwidth and T_a the total time record length. Substituting the appropriate values for B (2 Hz) and T_a (150 sec) gives $\epsilon = 0.25\ dB$. Thus the limits of error in measuring the sound intensity are approximately equal to the inherent statistical fluctuations (for frequencies above 100 Hz).

5.3 Length and Frequency Scaling

The three significant length scales for this experiment were:

1. the streamwise orifice dimension, b

2. the turbulent boundary layer thickness, δ, above the orifice, and

3. the lateral correlation length, ℓ.

Table 2 provides the applicable values for b, δ and ℓ used in this experiment. The lateral correlation length ℓ was inferred from existing transverse cross-spectra of wall pressure beneath turbulent boundary layers (see Appendix 3).

Orifice/ Louver	b(cm)	U(m/s)	ℓ (cm)	δ(cm)	δ/b for O-2	δ/b for O-3
O-1	4.23	20	2.4	4.19	0.99	3.95
O-2,/O-2A	4.23	30	1.8	3.86	0.91	3.64
O-3,/O-3A	1.07	40	0.9	3.65	0.86	3.44
L-1,/L-1A	1.07	50	1.4	3.49	0.83	3.29
L-2,/L-2A	1.07	50	2.1	3.49		
Full Scale	2.50	16.5		4.70	1.88	

Table 2: Experimental Length Scales

Note: Full scale assumes a louver positioned 15 ft from the leading edge of a flat surface in seawater at 58 F. The louver consists of multiple rectangular shaped openings, each of transverse dimension, $b = 2.5\ cm$. From Figure 16 at $\delta/b = 1.88$, the Strouhal # = 0.19. Therefore the full scale frequency, f_c, is:

$$f_c = (0.19)(16.5)/(0.025) = 125\ Hz$$

32

The significant frequency scales were the non-dimensional strouhal numbers $St(b)$ and $St(\ell)$ defined by:

$$St(b) = f_c b/U_\infty$$
$$St(\ell) = \omega \ell/U_c = 4\pi f_c \ell/U_\infty \qquad (5.2)$$

where f_c is the center frequency of the 1/3 octave band with the peak sound power level. Figure 14 is a graph of f_c versus U_∞ for orifice $0 - 1$ at a constant b. The data points reflect several separate experiments measuring the sound pressure level at radial distances of 9, 18, 24 and 36 inches from the orifice. Figure 15 plots f_c versus U_∞ for orifices $0 - 1, 0 - 2, 0 - 3$ and louver $L - 1$ and $L - 2$. Clearly there exists a linear relationship (or nearly linear) between f_c and U_∞ for a particular transverse dimension b.

Table 3 lists the non-dimensional Strouhal numbers for the above orifices/louver as well as the non-dimensional length scale, δ/b for $U = 20$ m/s. The strouhal number, $St = fb/U$, has been defined to equal that recommended by DeMetz and Farabee [5] to compare results. Figure 16 is the graph of the data in Table 3 along with the results of DeMetz and Farabee [5] for TBL flow over orifices enclosed by solid cavities.

Orifice/ Louver	$St(b) = fb/U$ Strouhal #	Non-dimensional length scale δ/b
O-1	0.17	1.22
O-2	0.23	1.22
O-3	0.12	4.79
L-1	0.076	4.79
L-2	0.048	4.79

Table 3: Non-dimensional Frequency and Length Scales at $U = 20$ m/s

The decreasing trend in the Strouhal number with increasing δ/b for the two cases agrees reasonably well. Having a knowledge of the boundary layer thickness, one can enter Figure 16 at the appropriate value for δ/b and determine
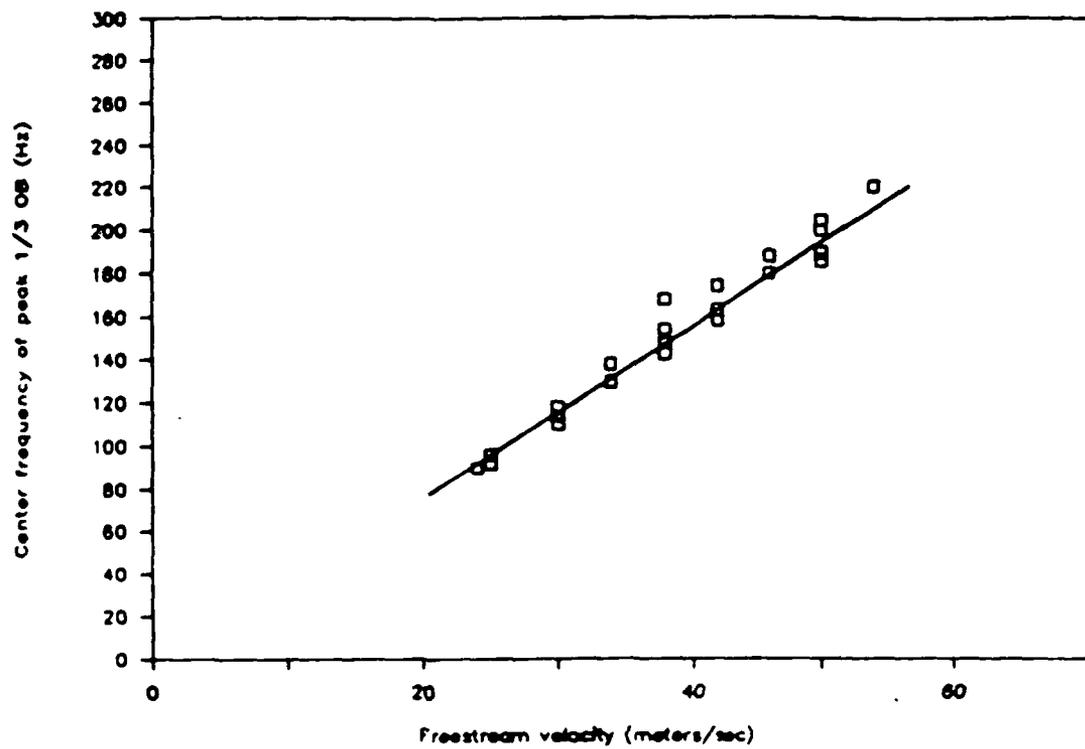
Figure 14: Frequency/velocity relationship for orifice O1. Shown are four separate experiments for various radial distances, r.
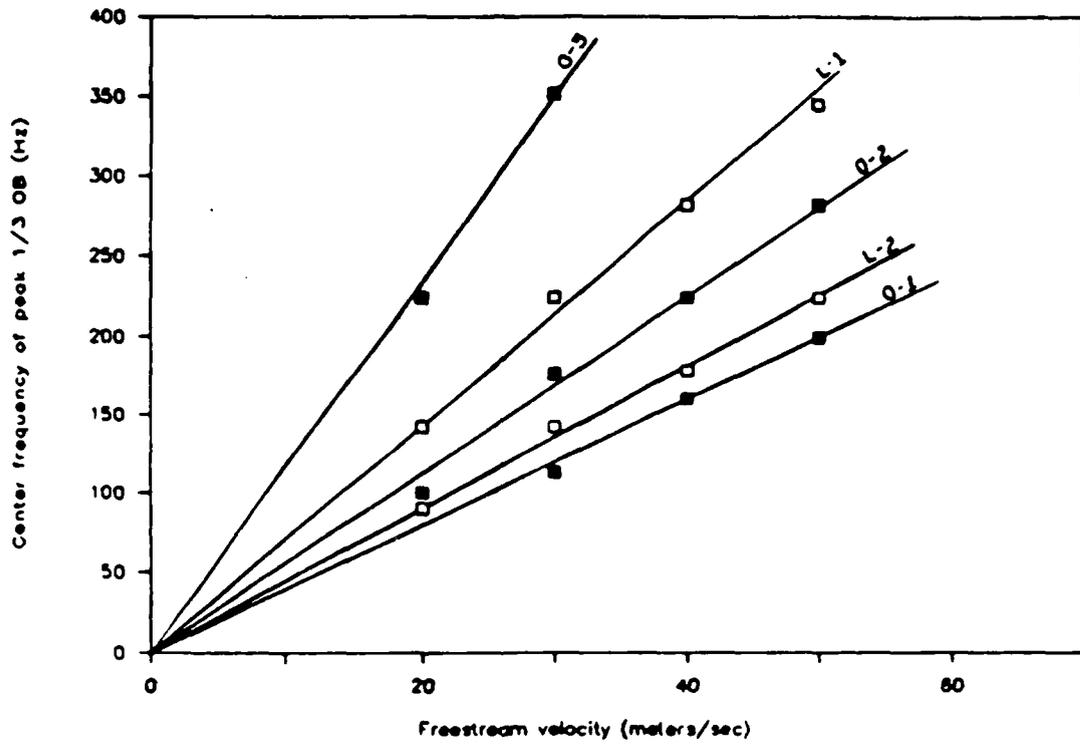
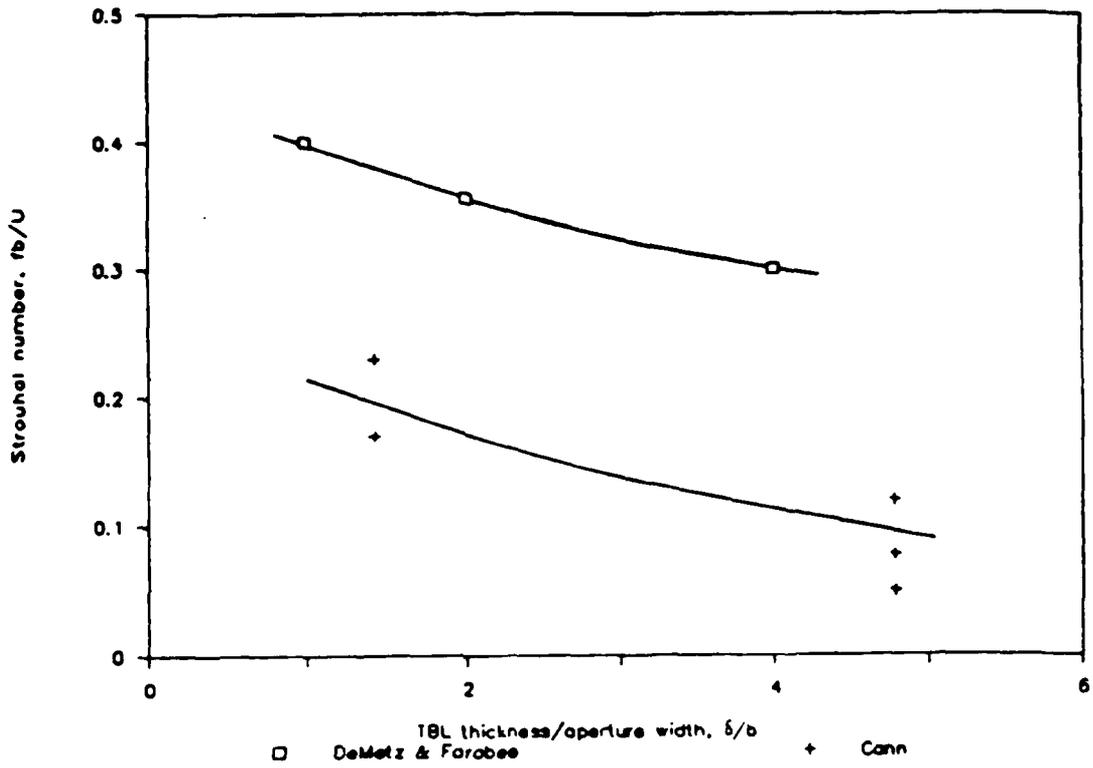Figure 15: Frequency/velocity relationships for orifices $O1, O2, O3$ and louvers $L1, L2$

Figure 16: Strouhal number versus boundary layer/aperture width ratio

36

the Strouhal number for orifice or louver flow noise. From the Strouhal number and the geometry of the aperature(s), one can predict f_c.

5.4 Structural Radiation Due to TBL Excitation

To determine the contribution from structural radiation caused by the excitation from the TBL, an experiment was conducted at all free stream velocities with the orifice/louver covered. Identical sound power spectrums were recorded as described in Section 4.1. The resulting background power spectrums levels, Figures 17, 18, 19 and 20, were 10 to 46 dB lower than with the orifice exposed. From these figures, the major contribution from the orifice/louver sources was in the range of 65 to 1000 Hz. Background noise was within 15 dB of the orifice/louver noise below 50 Hz and above 1000 Hz.

5.5 "Open Window" Contribution

Previous work by Spinka [15] determined the acoustic pressure field within the test section at various free stream velocities. To determine the contribution from the open window affect, a similar acoustic pressure field was generated within the duct using a speaker driven a B & K random noise generator, type 1402, and a B & K band pass filter set, type 1612. The resulting power which radiated through the orifice was measured as described in Section 2.5 and compared to the power radiated by the orifice source. Table 4 lists the resulting power levels for both cases at $U = 50 \ m/s$. The conclusion was that the open window affect results in levels which were typically 23 dB lower than the levels due to the orifice source.

1/3 OB center frequency	Open window power in 1/3 OB (2)	Orifice O-1 power in 1/3 OB (3)	(3-2)
400	53.8	77.6	23.8
500	48.2	72.7	24.5
630	45.9	69.2	23.3
800	43.7	67.9	24.2
1000	46.2	66.4	20.2
1250	41.0	64.5	23.5

Table 4: "Open window" power levels versus orifice O -1 power levels at $U = 50 \ m/s$

5.6 Orifice Source Power Spectra and Total Power

The measured sound power spectra versus the free stream velocity, $U = 20, 30, 40$ and $50 \ m/s$, for $O - 1, O - 2, O - 3, L - 1$ and $L - 2$ are shown in

Figures 21, 22, 23, 24, 25. The total sound power radiated by each orifice/louver source at the above speeds is given in Table 5.

37
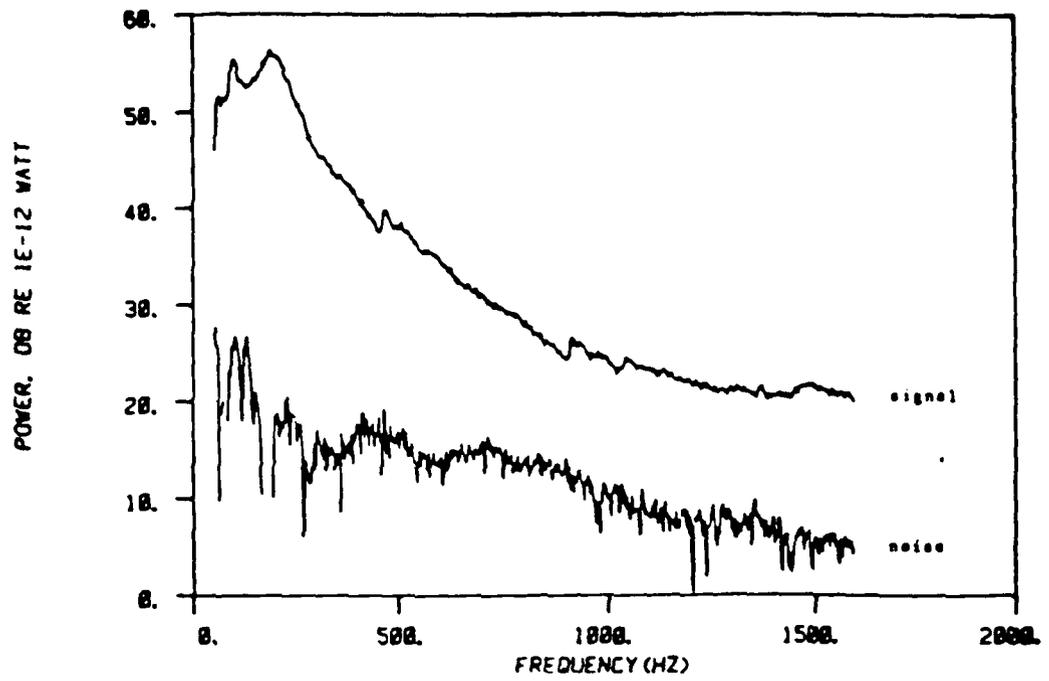
Figure 17: Signal to noise for orifice O1 at $U = 30\ m/s$.

38
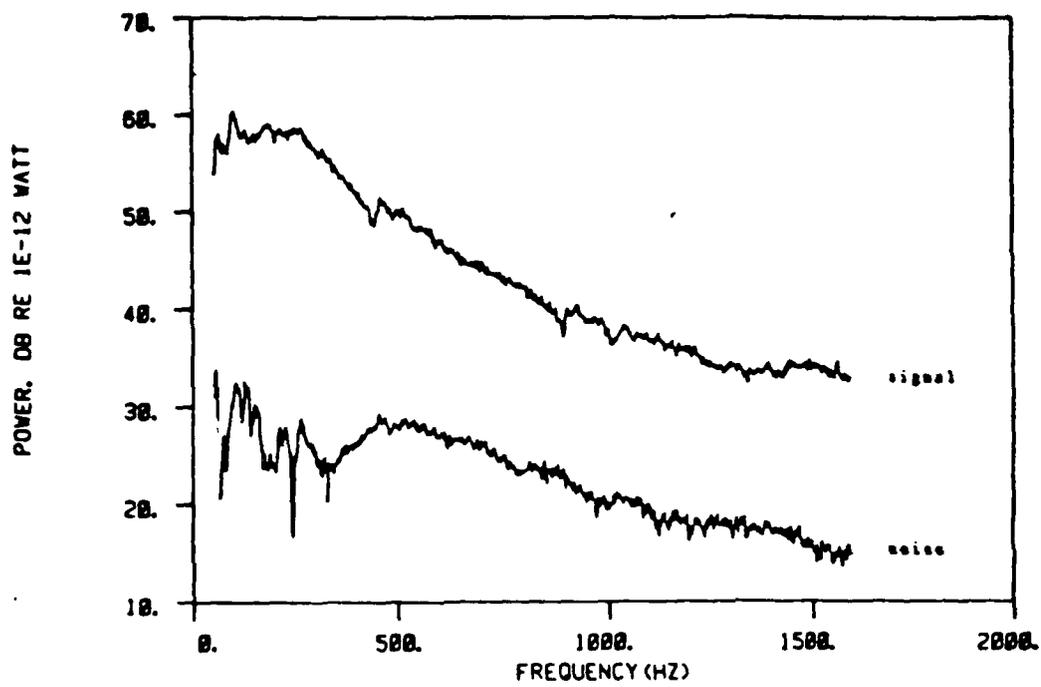
Figure 18: Signal to noise for orifice O2 at $U = 40 \; m/s$.
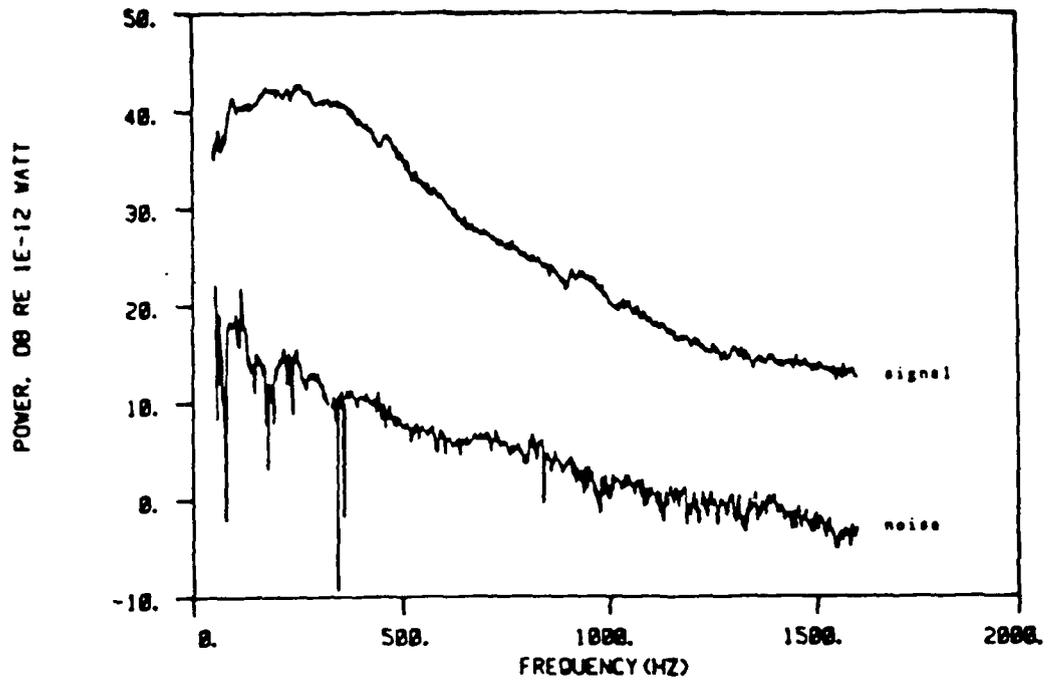
Figure 19: Signal to noise for orifice O3 at $U = 20 \ m/s$.
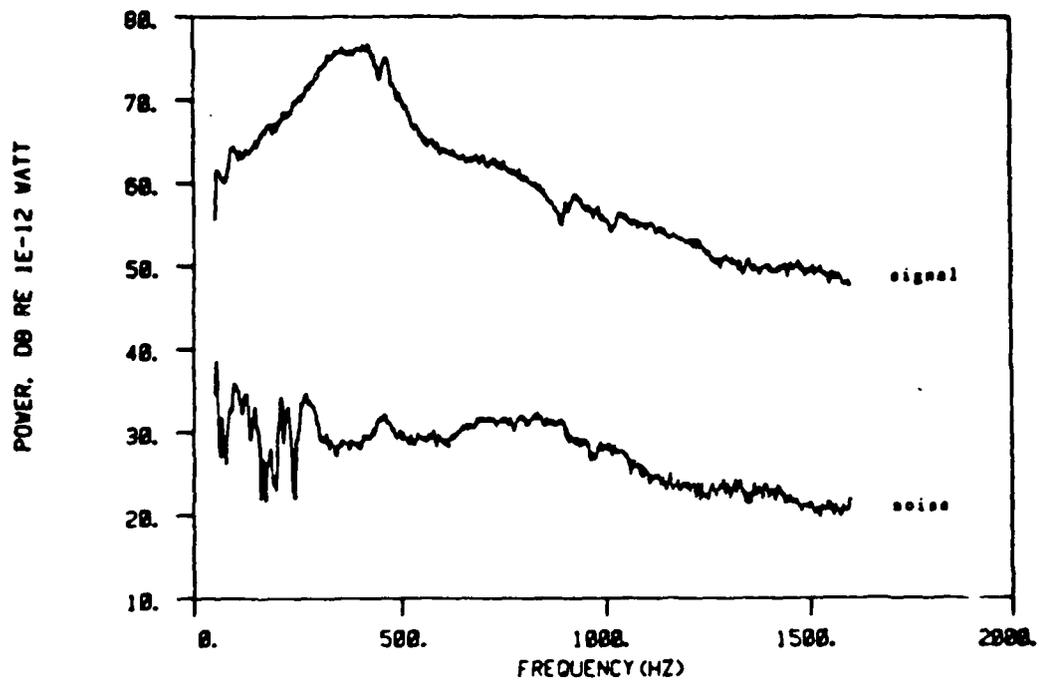
Figure 20: Signal to noise for louver $L1$ at $U = 50 \; m/s$.

41

Figure 21: Orifice O1 sound power spectral level versus free stream velocity

Figure 22: Orifice O2 sound power spectral levels versus freestream velocity
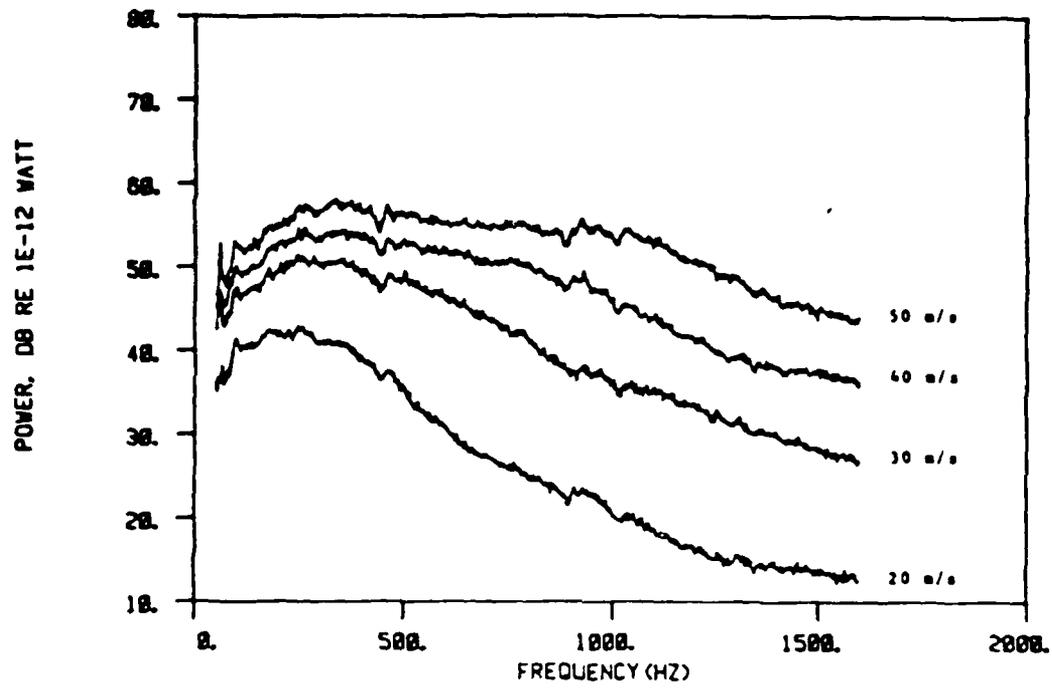
Figure 23: Orifice O3 sound power spectral levels versus freestream velocity

44
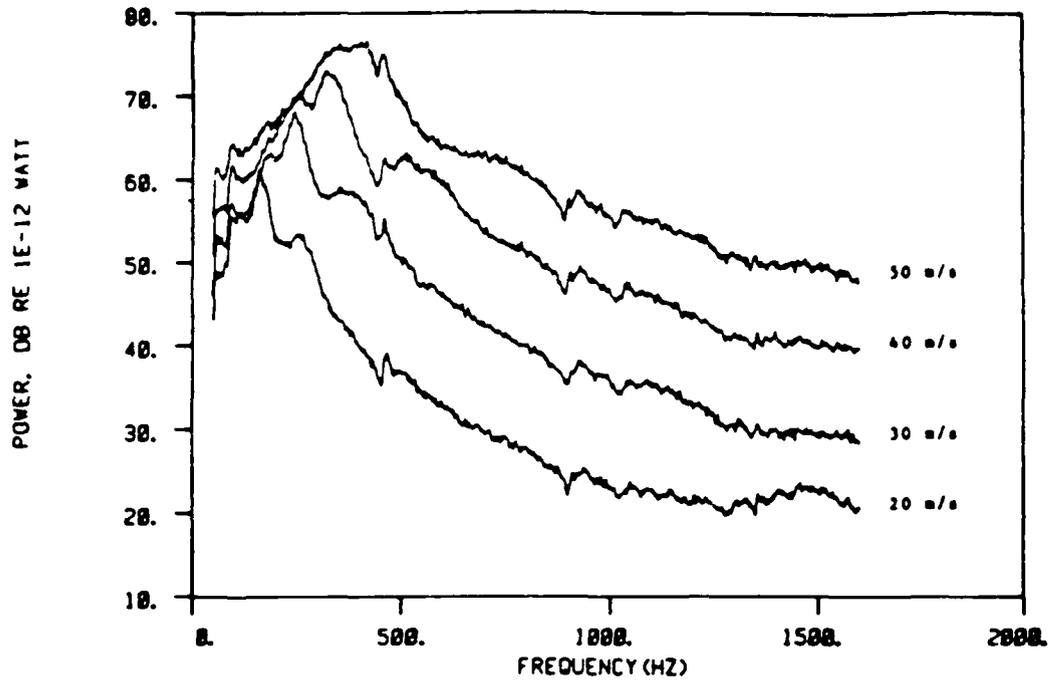
Figure 24: Louver L1 sound power spectra levels versus freestream velocity
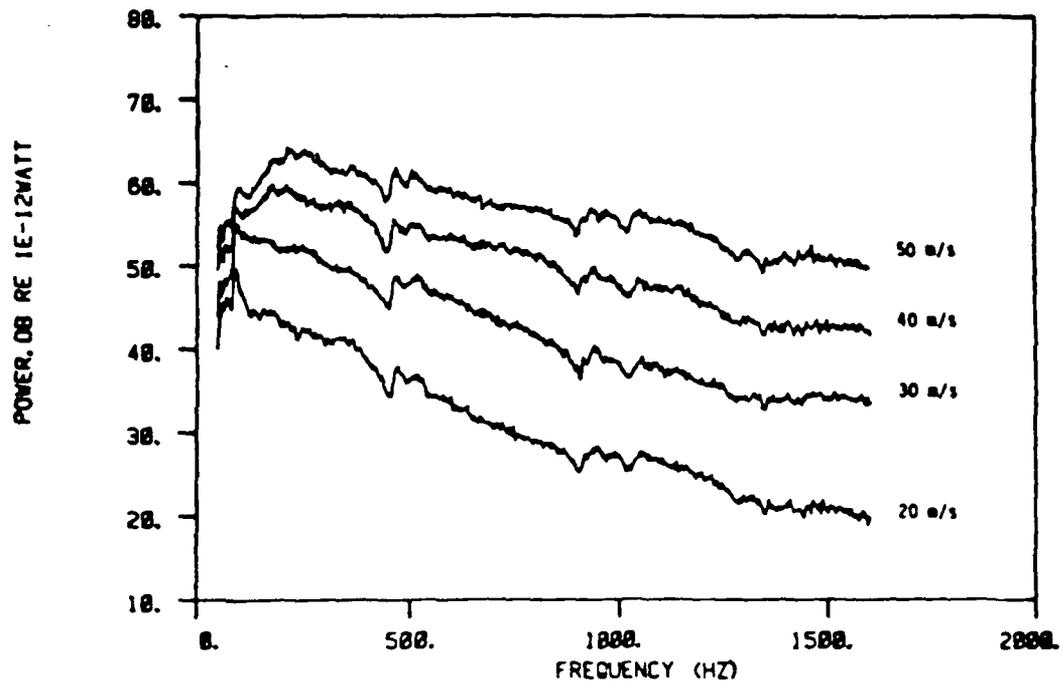
Figure 25: Louver L2 sound power spectral levels versus freestream velocity

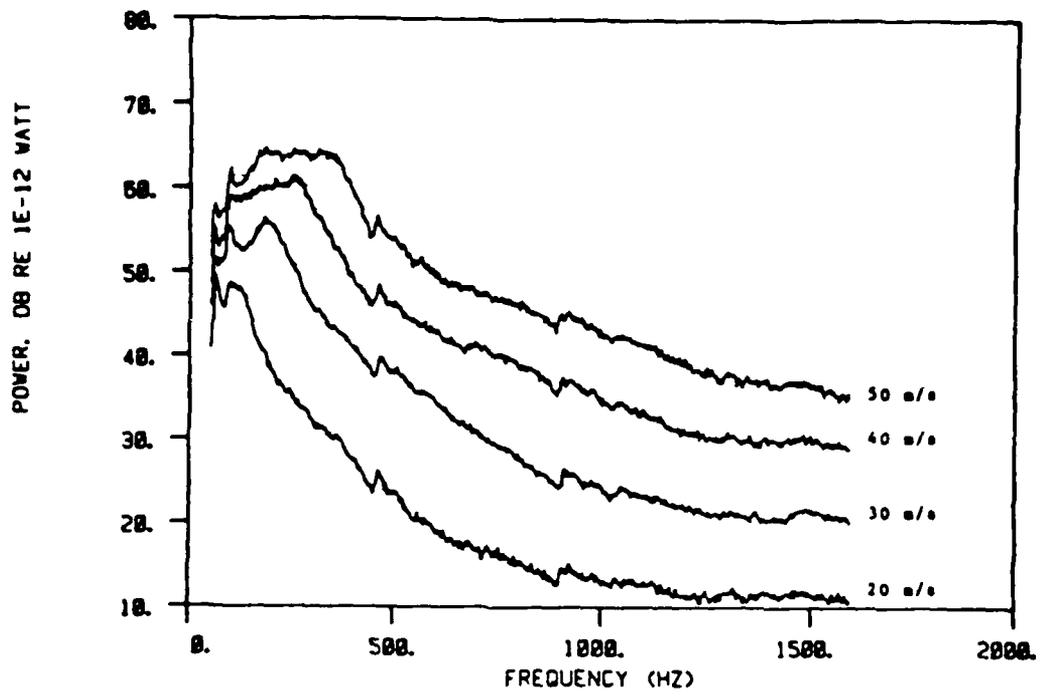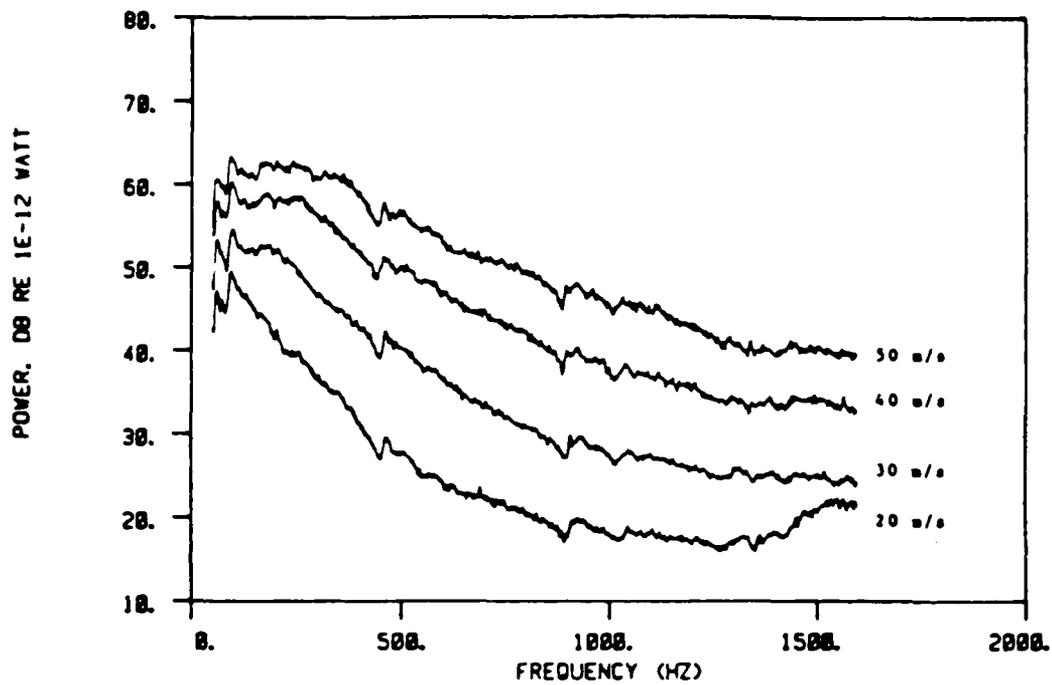| Orifice/ Louver	Free Stream Velocity U(m/s)	Total Sound Power (dB re 1 E-12 watts)
O-1	20	63.3
	30	73.3
	40	79.6
	50	84.0
O-2	20	62.7
	30	73.2
	40	78.4
	50	83.0
O-3	20	62.9
	30	72.2
	40	76.3
	50	79.7
L-1	20	74.5
	30	82.5
	40	89.2
	50	94.5
L-2	20	64.9
	30	73.6
	40	80.1
	50	85.3
O-2A	20	62.0
	30	71.8
	40	77.2
	50	82.2
L-1A	20	58.1
	30	68.4
	40	73.3
	50	77.7
L-2A	20	55.3
	30	65.0
	40	69.7
	50	76.3

Table 5: Orifice/louver total sound power levels versus freestream velocity, U_∞

Several observations are made from reviewing the above data.

5.6.1 The effect of louvering on sound power

- louver, L-1, radiated the most acoustic power, averaging 10 dB more at all speeds than the single orifice though the total open areas were the same (see Figures 26 and 27).

- louver, L1, showed strong resonant peaks and had the narrowest half-power bandwidth of all the samples tested.

47
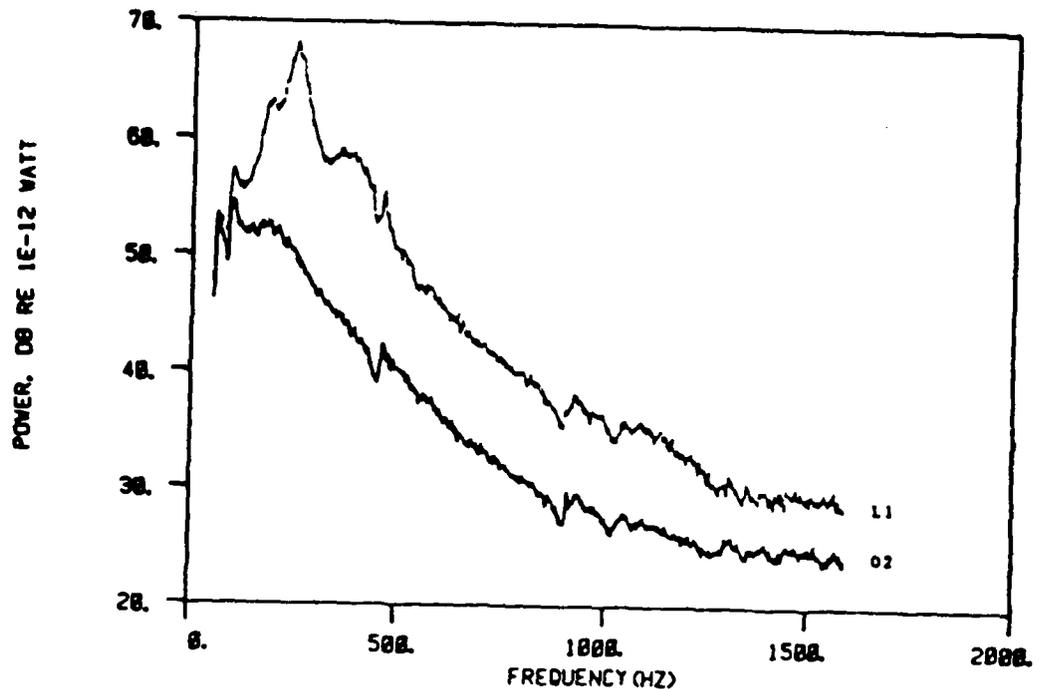
Figure 26: The effect of louvering on sound power, $L1$ versus O2 at $U = 30 \ m/s$

- louver, L1, radiated significantly more power than louver L2 in the lower frequency bands but approximately equal power in the middle to high frequency bands (see Figures 28 and 29)

- louver, L2, had the broadest spectra of all the samples tested with equal open area.

- louver, L2's total radiated power was within 2 dB of orifice O2's power in all speed ranges but the spectral shape was significantly broader. As shown in Figures 30 and 31, louver L2 radiated significantly more power than O2 in the middle to higher frequency bands (10 dB more on average) but slightly less (approximately 1-2 dB) power in the lower frequency bands.

Thus the effect of louvering, simply by dividing the total open area into more numerous, smaller areas does not by itself reduce the total radiated flow noise and will most probably result in increased radiated sound power in the higher frequency bands.

48
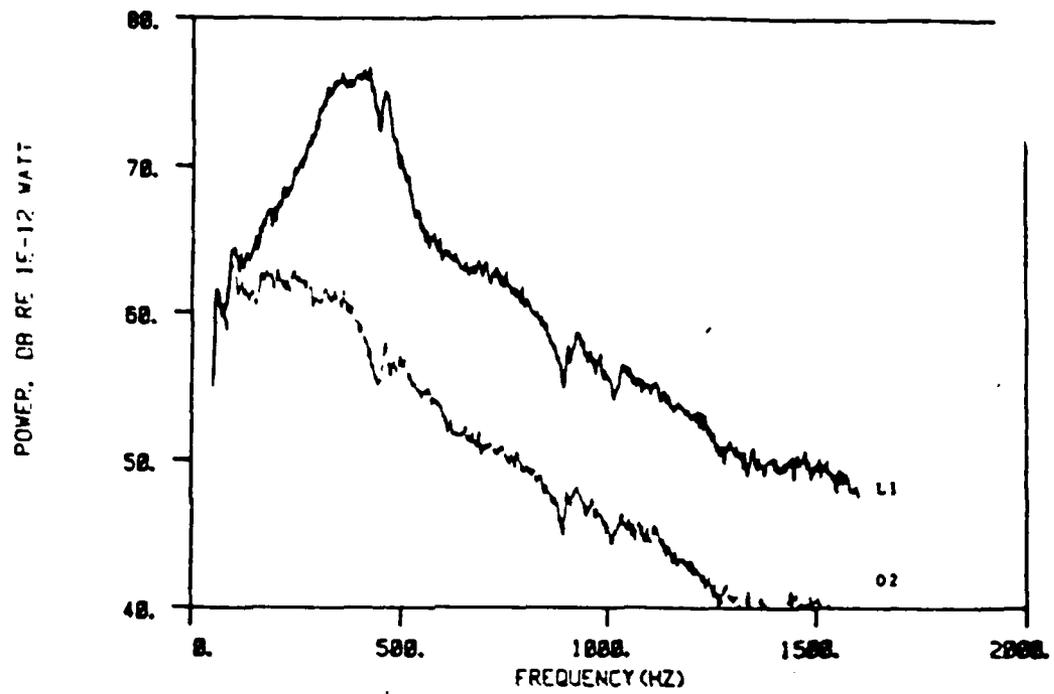
Figure 27: The effect of louvering on sound power, $L1$ versus O2 at $U = 50\ m/s$

49
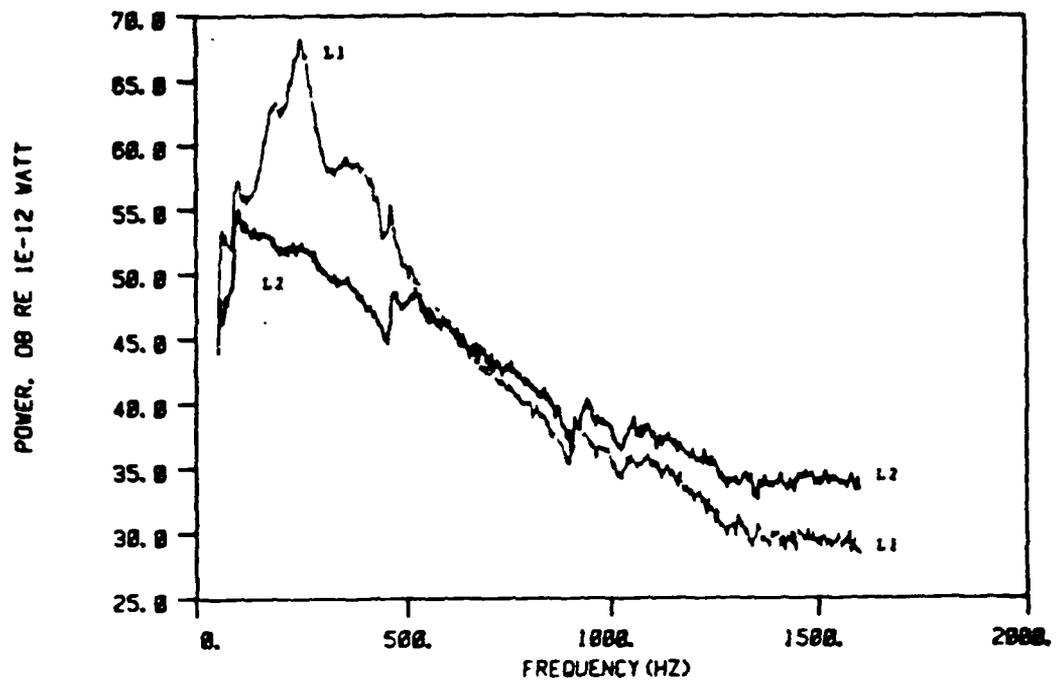
Figure 28: Louver geometry effect on sound power, $L1$ versus L2 at $U = 30\ m/s$
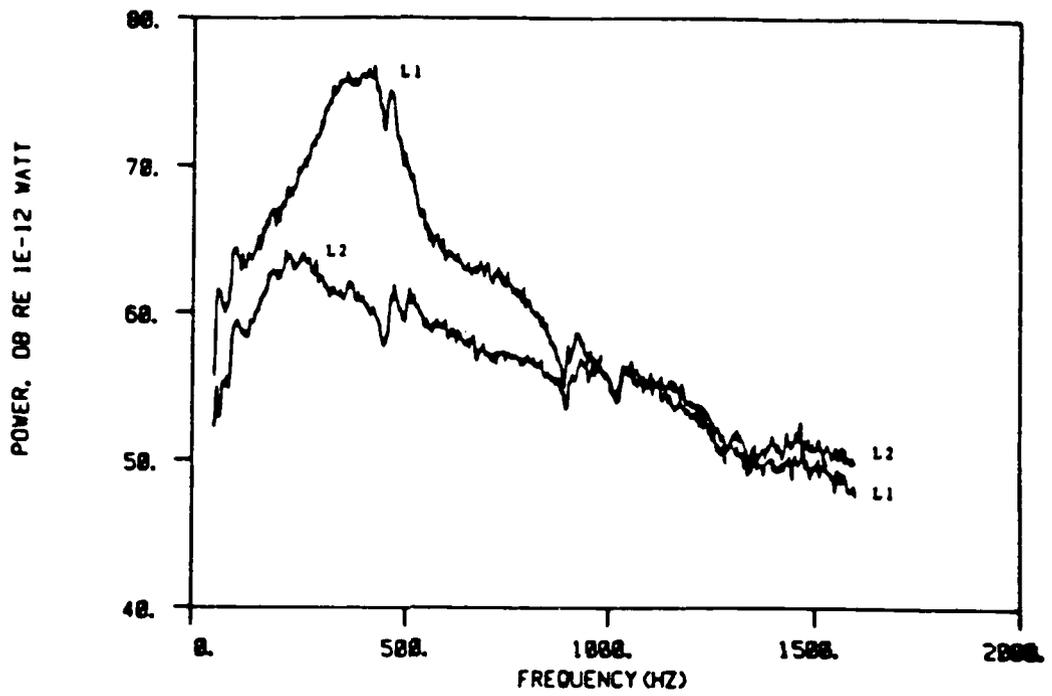
Figure 29: Louver geometry effect on sound power, $L1$ versus L2 at $U = 50\ m/s$
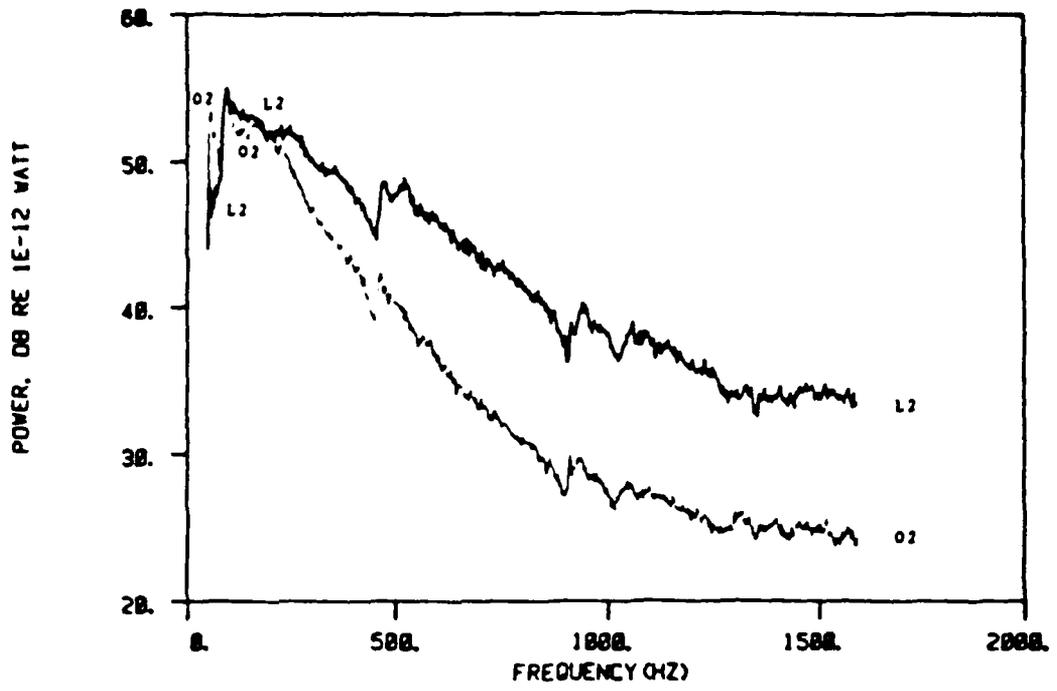
Figure 30: Effect of louvering on sound power, $L2$ versus O2 at $U = 30 \ m/s$
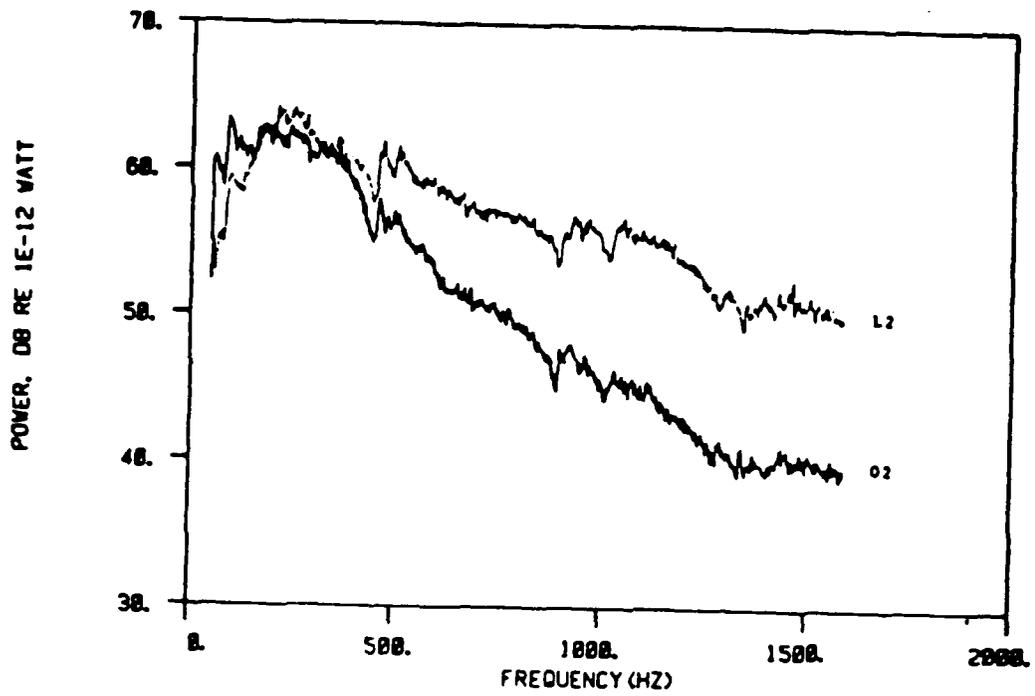
Figure 31: Effect of louvering on sound power, $L2$ versus O2 at $U = 50 \ m/s$
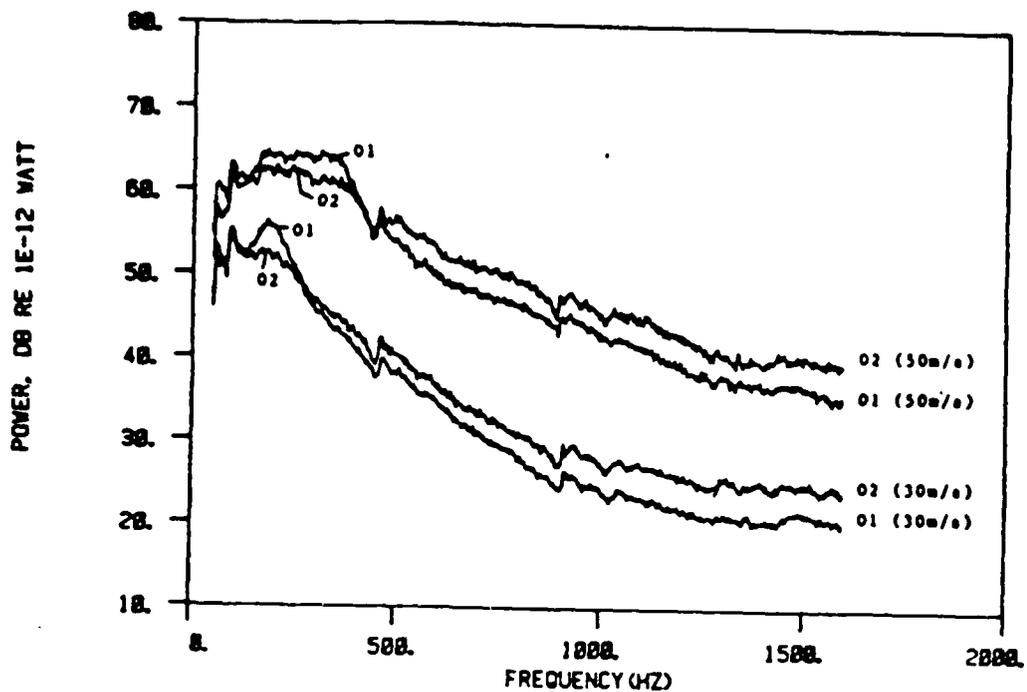
Figure 32: Orifice depth effect on sound power, O1 versus O2 at $U = 30$ and 50 m/s

5.6.2 Orifice throat thickness effect on radiated power

Figure 32 shows the orifice throat depth effect on sound power by comparing orifice O1 to orifice O2. Orifice O2 radiated more power (approximately 3dB) in the higher frequency bands but maintained approximately 1-2 dB less power in the more dominant lower frequency bands.

Thus the throat thickness was more predominant in effecting the spectral shape than reducing the total radiated power. The effect of reducing the orifice throat thickness appears to broaden the spectral shape while maintaining the same total radiated sound power.

5.6.3 Streamwise dimension, b, effect on sound power

The spectral shape of orifice O3 had the widest half-power bandwidth. The effect of reducing the streamwise dimension, b, was to broaden considerably the

power spectra while reducing only moderately the total sound power. From section 3, the controlling shape factor was (1-cos(Kb)). Thus the predicted result from reducing b by four fold would be a subsequent increase by four fold in the power spectra bandwidth. Reviewing again the power spectra for orifices O2 and O3 (Figures 22 and 23), we see that indeed the power bandwidth for O3 is approximately four times that of O2 (defining the bandwidth to be between the one-quarter peak spectral power points).

5.7 Speed/Power Laws

The speed/power law is of the form:

$$P = CU^n$$

where C is a value which is independent of speed. The data in Table 5 was utilized to determine the total radiated power dependence on speed. The equations used to determine the value of the speed exponent, n, were:

$$P_3/P_2 = (U_3/U_2)^n$$

$$10\log(P_3/P_{ref}) - 10\log(P_2/P_{ref}) = n\ 10\log(U_3/U_2)$$

$$L_{p_3} - L_{p_2} = n\log(U_3/U_2)$$

$$n = (L_{p_3} - L_{p_2})/(10\log(U_3/U_2))$$

where the subscripts 3 and 2 correspond to 30 and 20 m/s. Similar equations hold for U_4/U_2, U_5/U_2, U_4/U_3, U_5/U_3 and U_5/U_4. Table 6 lists the calculated value for n for each sample tested. The values for n varied from 3.3 to 6.8 with a mean value of 4.9 and a standard deviation of O.3. Excluding the extremely low values of n recorded for 03 at the higher free stream velocities, the mean value of n was 5.0 with a standard deviation of 0.2.

55

The speed/power relationship for orifices $O1$, $O2$ and louvers $L1$ and $L2$ is plotted in Figure 28. Also shown is the least squares fit to the data points satisfying the equation:

$$(Lp_i - LP_j) = n10 \ \log(U_i/U_j) \qquad (5.2)$$

From the fit, the best value for n is 4.97.

Orifice/Louver	U_3/U_2	U_4/U_2	U_5/U_2	U_4/U_3	U_5/U_3	U_5/U_4
O-1	5.7	5.4	5.0	5.2	4.8	4.5
O-2	6.0	5.2	4.2	5.1	4.4	4.7
O-3	5.3	4.5	3.3	4.2	3.4	3.5
L-1	4.6	4.9	5.4	5.0	5.4	5.5
L-2	4.9	5.2	5.5	5.1	5.3	5.0
O-2A	5.6	5.1	4.3	5.1	4.7	5.2
L-1A	5.9	5.1	3.9	4.9	4.2	4.5
L-2A	5.5	4.8	3.8	5.3	5.1	6.8
average	5.4	5.0	4.5	5.0	4.7	5.0
std. dev.	0.5	0.3	0.6	0.3	0.6	0.9
overall average 4.9		overall	standard	deviation	0.3	

Table 6: Speed/Power relationship $(P = CU^n)$, values for the speed exponent, n

Thus the concluding dependence is:

Total radiated power increases with the 5th power of the free stream velocity.

5.8 Directivity of orifice O1 and louver L2A

Directivity measurements from orifice O1 and louver L2A were taken at $U = 25 \ m/s$. Figure 24 details the coordinate system used for the measurements. The measurements indicated the source was nearly omni-directional. Power levels in the XZ (azimuth) plane deviated by 0.9 dB from the maximum level. In the YZ (polar) plane, power levels deviated by 2.6 dB from the maximum level. Off the major axis, power levels deviate by 3.6 dB from the maximum level directly above the orifice source. Table 7 lists the measured sound intensity in $dB \ re \ 1E - 12 \ watt/m2$ at a radial distance of $r = 27$ inches and the various polar and azimuth angles. Figure 35 is the azimuth directivity plot for orifice O1 and louver L2A and clearly supports the conclusion of a nearly omni-directional source.
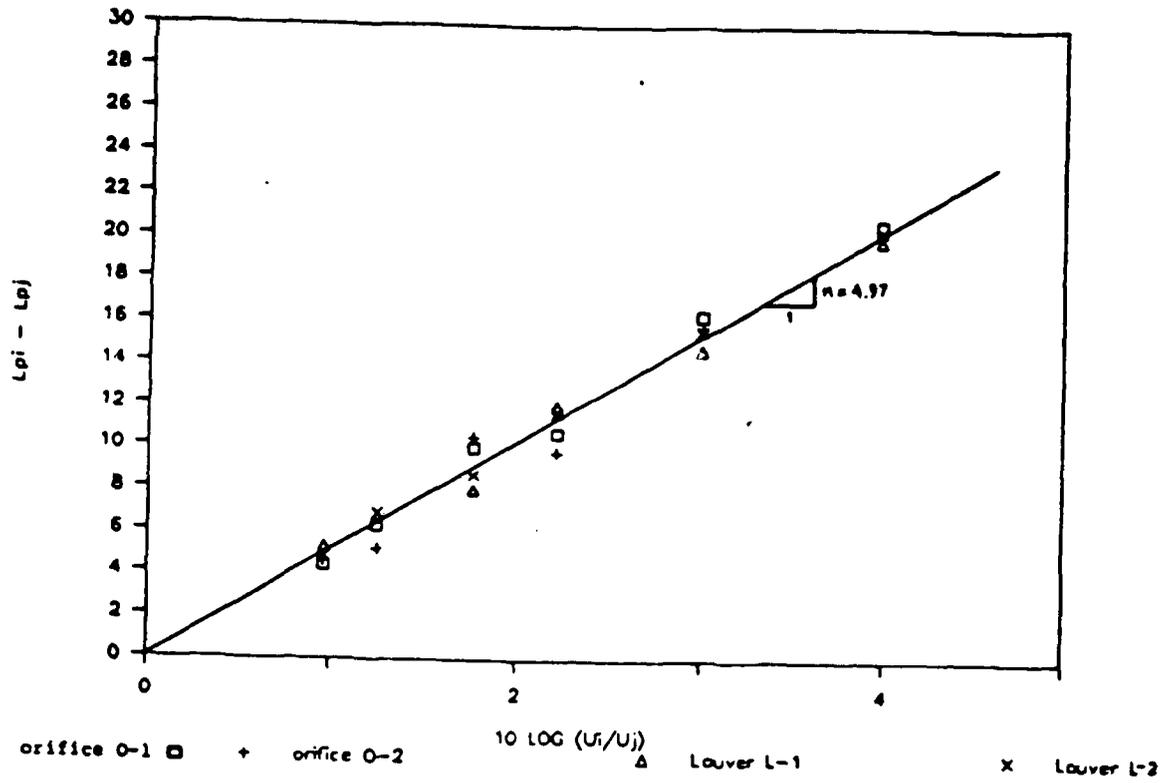
Figure 33: Speed/Power relationship for four samples $(P = CU^n)$ with least squares fit

Polar angle	Asimuthal angle Orifice 0-1	Total Intensity $dBre1E - 12\ watt/m^2$
0	90	57.3
0	45	56.9
0	15	56.4
0	135	57.1
0	165	56.8
0	105	57.2
0	75	57.0
-85	90	54.9
-45	90	56.5
0	90	57.5
45	90	57.0
85	90	55.9
-45	30	54.7
-45	25	53.9
-45	35	55.0
	Louver L-2A	
0	160	66.2
0	145	66.1
0	130	66.0
0	115	66.0
0	90	65.8
0	75	65.7
0	60	65.7
0	45	65.8
0	30	65.2
0	15	65.2
-90	90	63.4
-75	90	63.9
-60	90	65.0
-45	90	65.4
-30	90	65.9
-15	90	66.1
0	90	66.2
15	90	66.4
30	90	66.5
45	90	66.6
60	90	66.4
75	90	66.3
90	90	65.6
-45	45	65.3
-45	30	64.2
-45	90	65.3
-45	135	66.0

Table 7: Directivity measurement for orifice O-1 and louver L2A

58

Figure 34: Coordinate system for directivity measurements. Reference is the aperture center. Polar angle, θ, measured from Z axis, azimuthal angle, ϕ, measured from $-x$ axis. Measurements described by spherical coordinates, r, θ, ϕ.

5.9 Edge Angle Effect on Radiated Sound Power
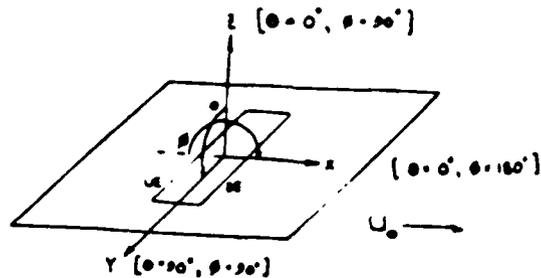
5.9.1 Introduction

Earlier it was shown that indeed the orifice source provided both the spectral character and the predominant amount of the total power. The strength of this source is due in part to the eddy interaction with the downstream edge of the orifice. To determine the relative importance of this edge interaction compared to the other significant parameters identified in Section 3, three additional orifice/louver samples were tested. They were orifice O-2A and louvers L-1A and L-2A. The details of these samples are described in Section 4. The only difference between these samples and the previously tested samples was the leading and trailing edges were slanted away from the flow by 40 degrees. This provided both a blunt orifice trailing edge where the eddies strike and a sharpened orifice leading edge (essentially reducing the upstream aperture to 1/32″, the radius of the edge).

5.9.2 Angled edge orifice/louver power spectra

The measured sound power spectra for the above samples are shown in Figures 31, 32, and 33. The total power radiated by each sample at the various freestream velocities is given in Table 5.
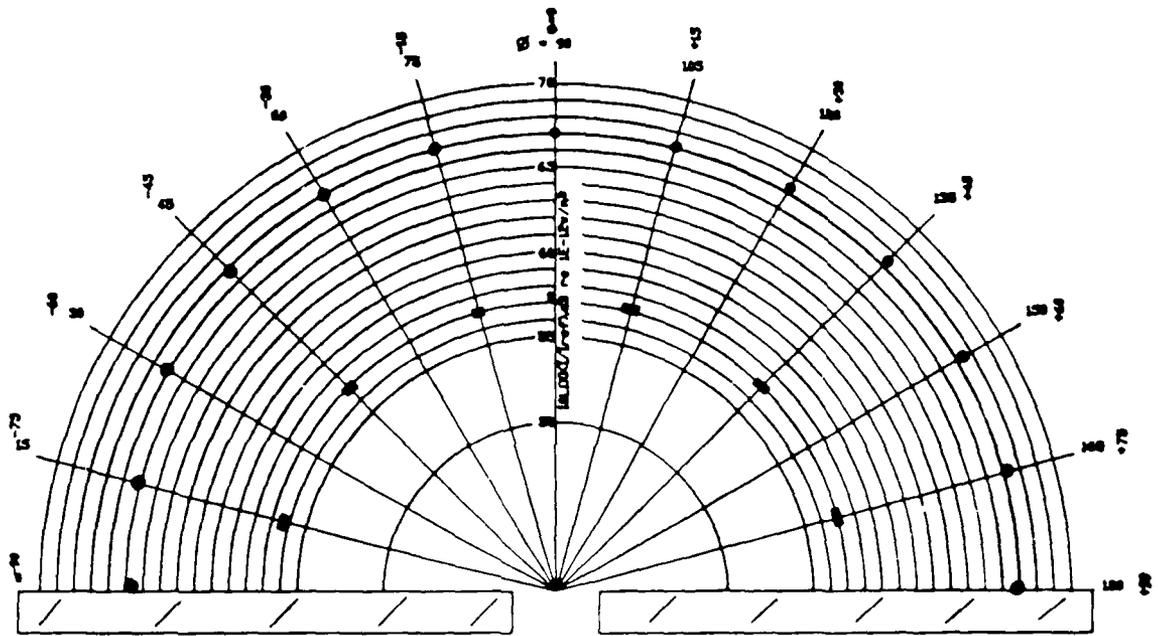
59

Figure 35: Orifice O1 directivity in the XZ (azimuth) plane and louver L2A directivity in the YZ (polar) plane

60
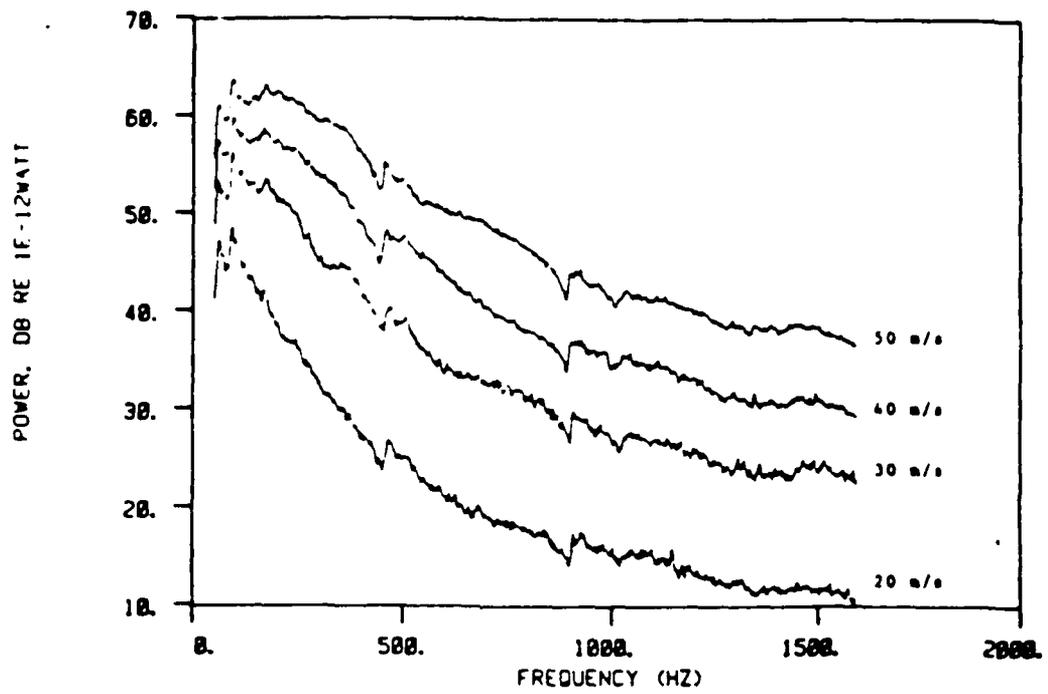
Figure 36: Orifice O2A power spectra level versus freestream velocity
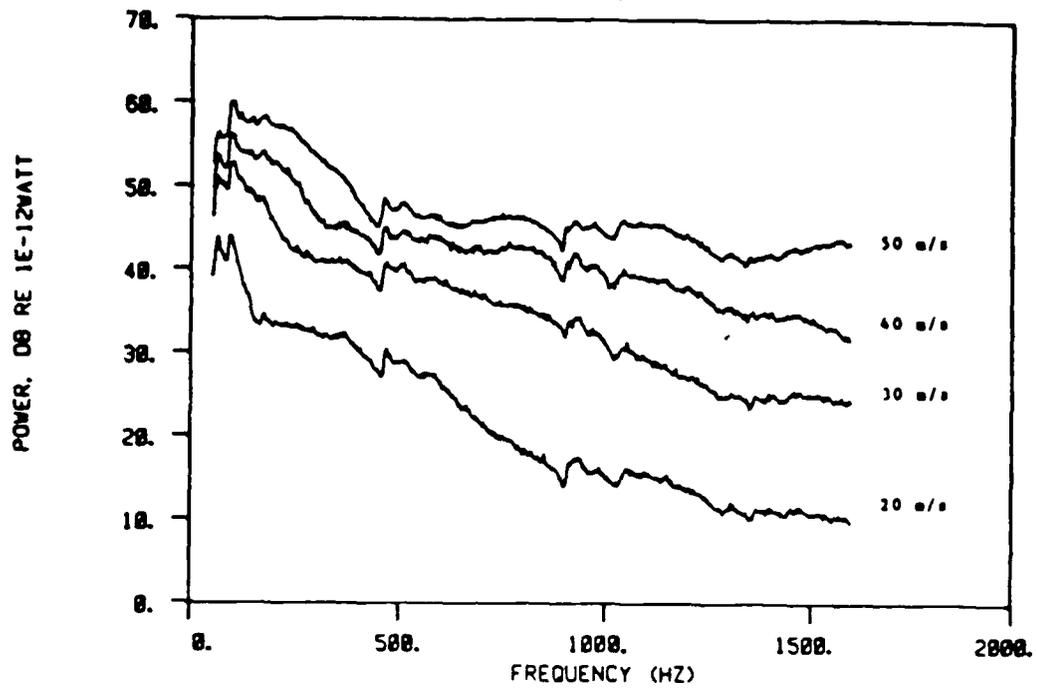
Figure 37: Louver L1A power spectral levels versus freestream velocity.

62
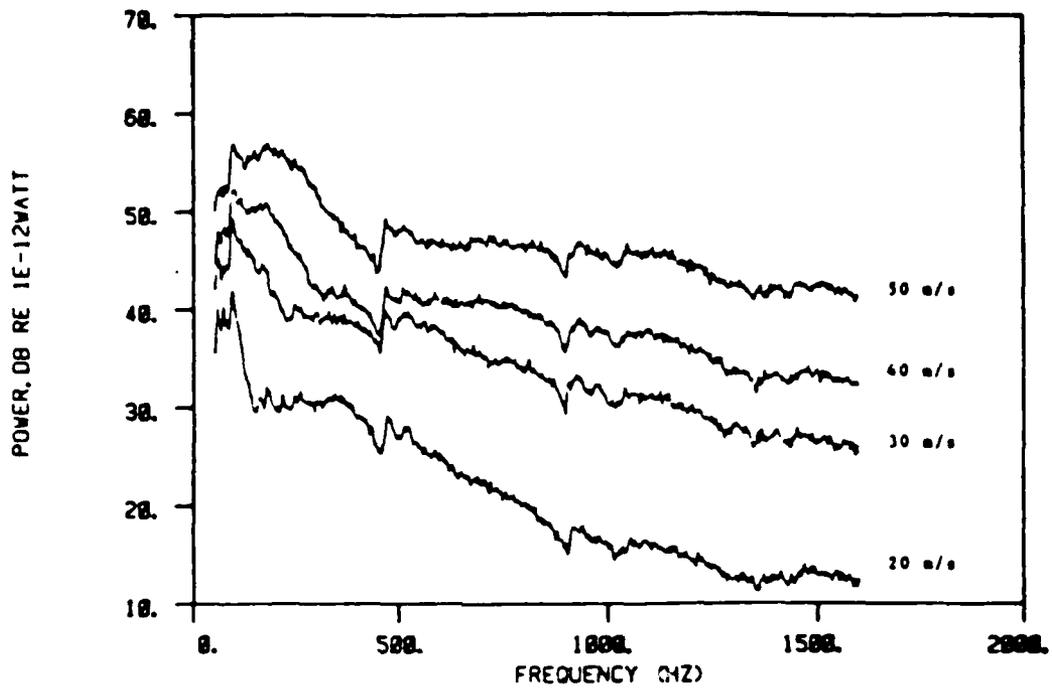
Figure 38: Louver L2A power spectral levels versus freestream velocity.
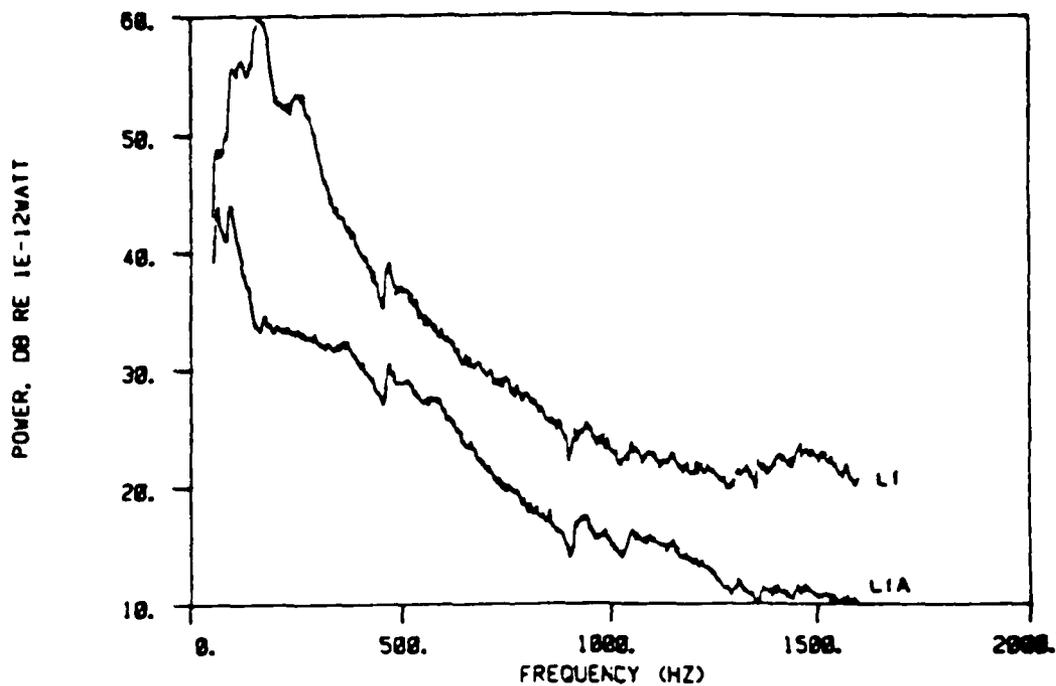
Figure 39: Edge angle effect on sound power spectral level, L1 versus L1A at $U = 20\ m/s$

Several observations are worth noting:

- the effect of angling the edges is more predominant for the louvers than the single orifice.

- the effect on louver L-1A is a 14-16 dB reduction in total radiated sound power. The large resonant peaks which occurred in the spectra for L-1 are not present in the spectra for L-1A. Figures 39 and 40 compare the two louvers at $U = 20$ and $50\ m/s$. Not only are the resonant peaks eliminated by angling the edges but also the radiated power is reduced by 5-7 dB in the higher frequency bands.

- Figure 32 compares the power spectral levels of L-2 and L-2A. The result for this louver is a 8.6 to 10.4 dB reduc tion in sound power equally divided across the frequency bands.

Figure 40: Edge angle effect on power spectral level, L1 versus L1A at $U = 50\ m/s$
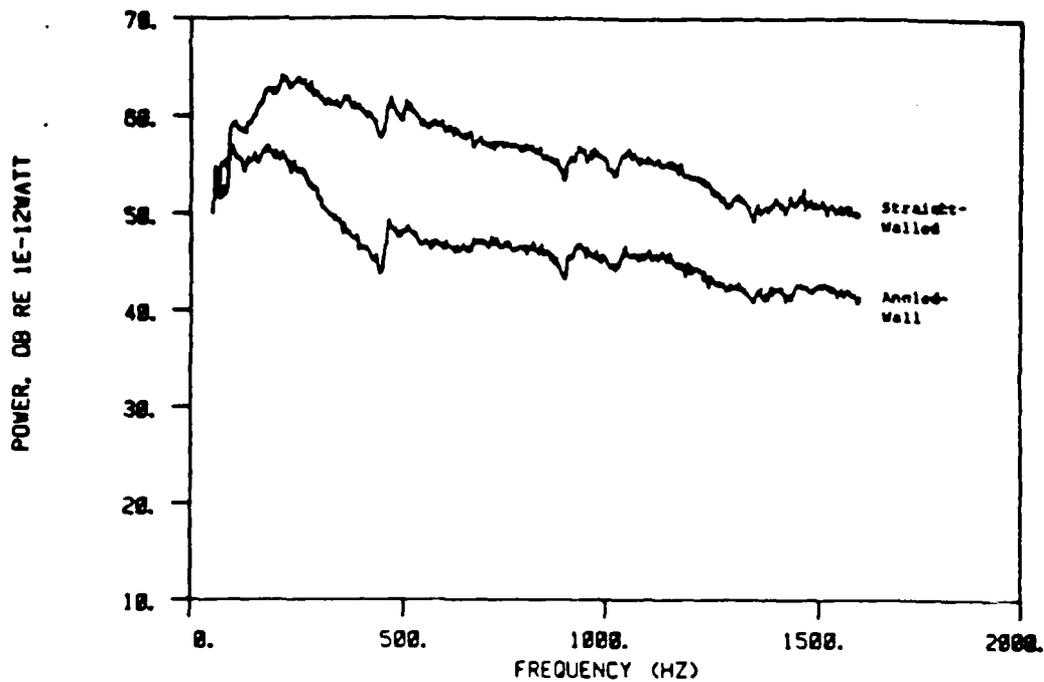
Figure 41: Edge angle effect on sound power spectral level, L2 versus L2A at $U = 50\,m/s$.

- for the single orifice, O-2A, the effect of angling the edges resulted in only a 0.7 to 1.4 dB reduction in sound power. Figures 33 and 34 compare the power spectra for orifice O-2 and O-2A at $U = 20$ and $50\,m/s$. Here again the effect of angling the edges resulted in a reduction in sound power in the higher frequency bands but in this case, essentially no change in the lower frequency bands.

5.9.3 Combined effect of louvering and angling edges

Taken together, the effect of louvering and angling edges results in a reduction of 3.4 to 7.5 dB in radiated sound compared to the single angled orifice (both of equal total open area). This reduction most probably is caused by two factors:

66
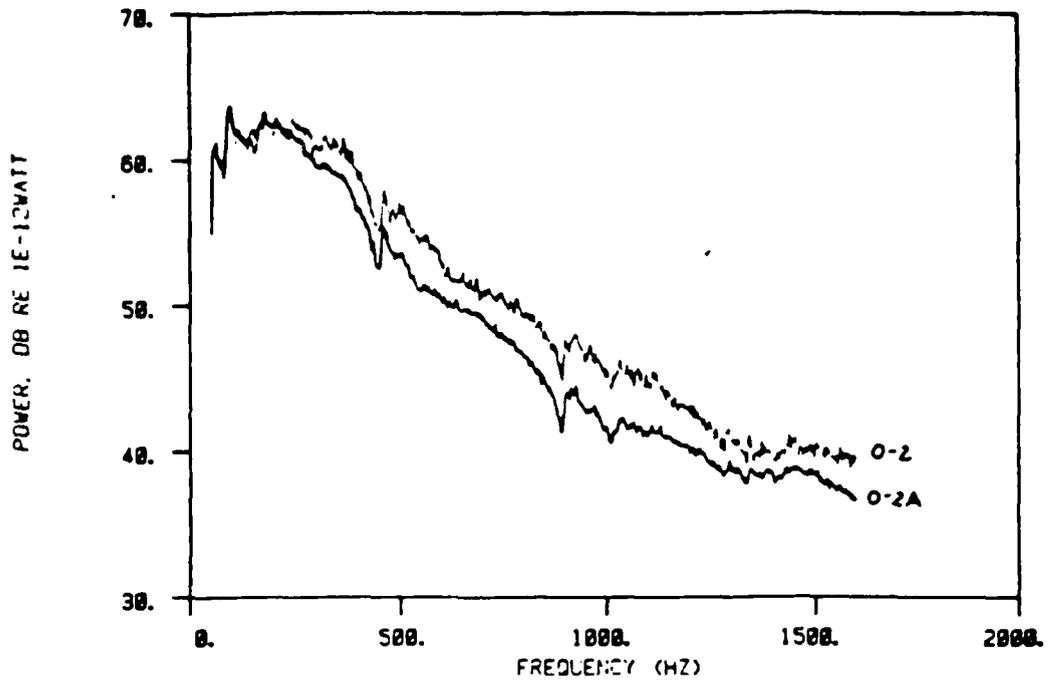
Figure 42: Edge angle effect on sound power spectral level, O2 versus O2A at $U = 50\ m/s$.
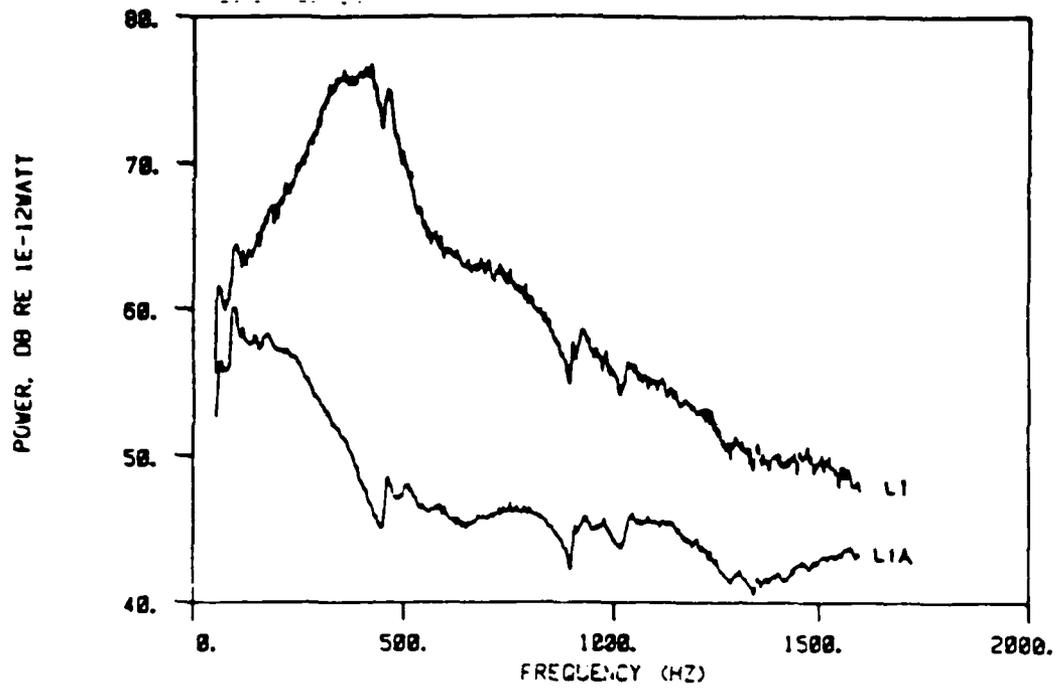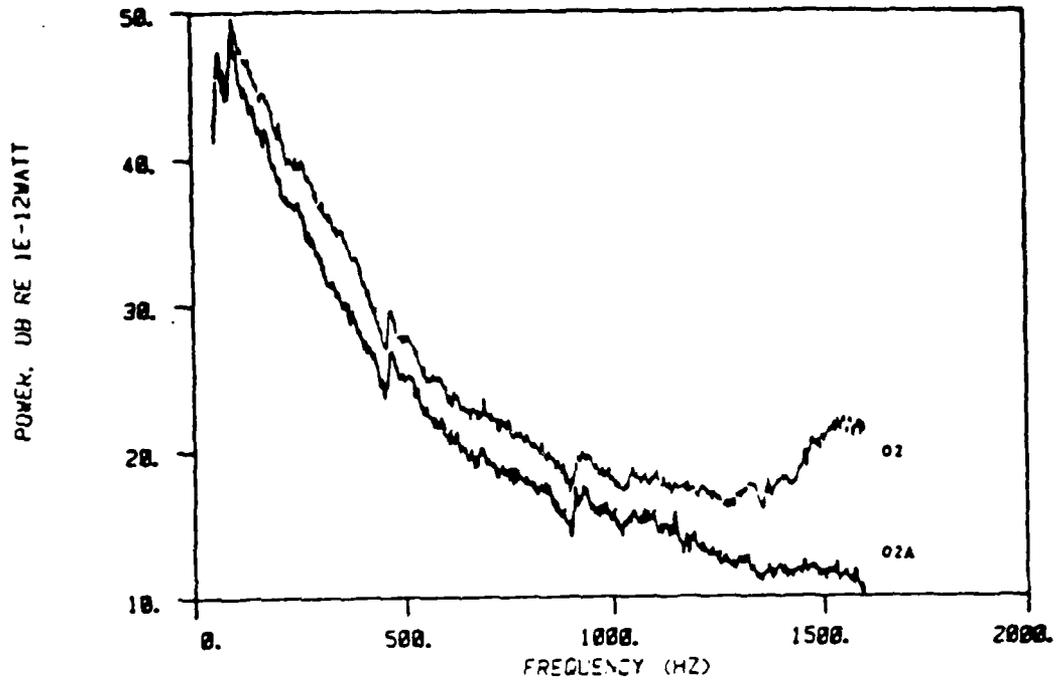
Figure 43: Edge angle effect on sound power spectral level, O2 versus O2A at $U = 20 \ m/s$.
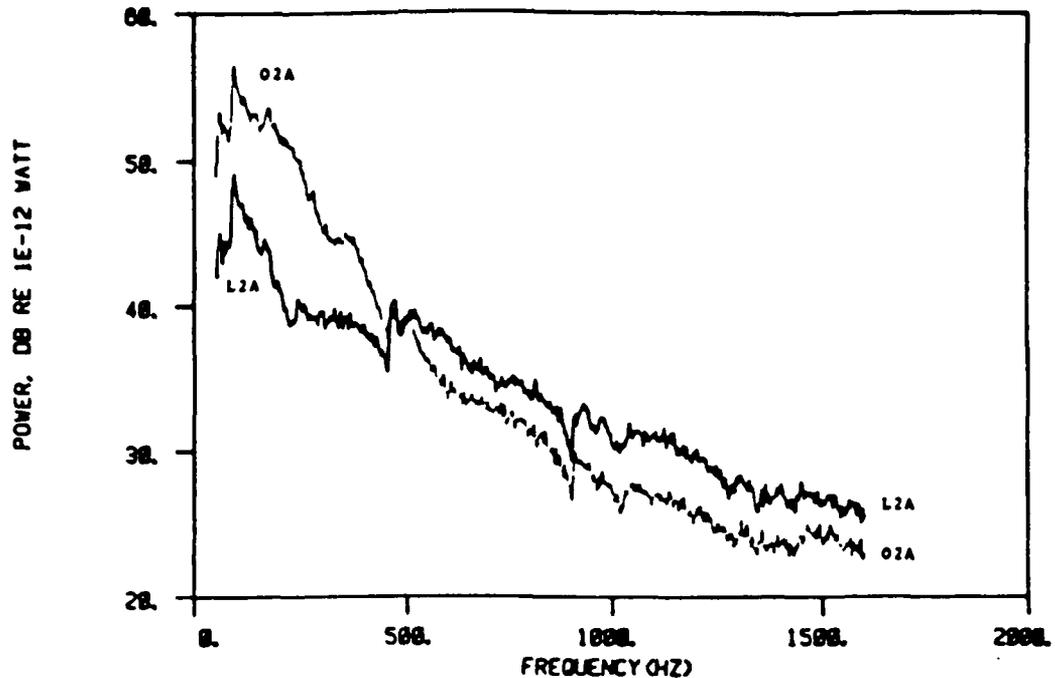
Figure 44: Effect of Louvering on sound power spectra level, L-2A versus O-2A at $U = 30\ m/s$

- the louvers shed eddies which after convecting downstream to the trailing edge are the same order in size as the edge thickness. This results in a more beneficial interaction when the eddies impact the angled edge. The orifice, however, with a four times larger aperture, sheds eddies which are much larger in size upon impact with the trailing edge and are therefore less affected by the thin angled edge.

- louvering, by reducing the transverse dimension, b, interferes with the longitudinal correlation of the shed eddies. This interference will be more predominant in the lower frequencies where the longitudinal correlation length is larger than the aperture transverse dimension, b. As shown in Figures 35, 36, 37, and 38, the reduction in sound power is predominantly in the lower frequency bands. There is, however, more radiated power in the angled louver in the higher bands by approximately 1-3 dB.

69

Figure 45: Effect of louvering on sound power spectral level, L-1A versus O-2A at $U = 30\ m/s$

Figure 46: Effect of louvering on sound power spectral level, L-2A versus O-2A at $U = 50\ m/s$

71
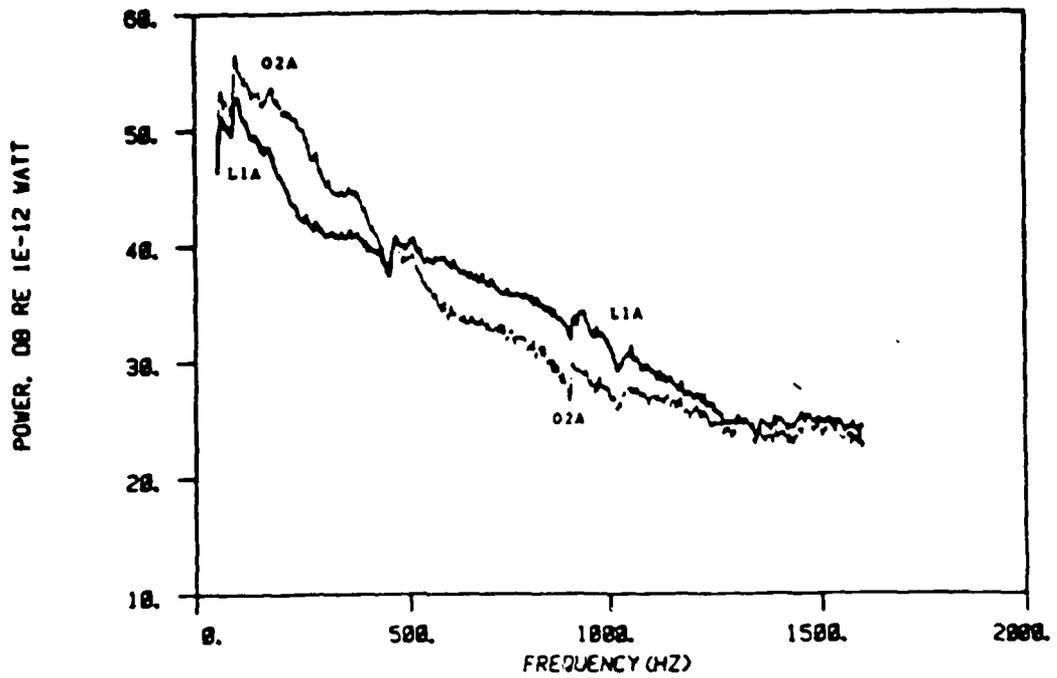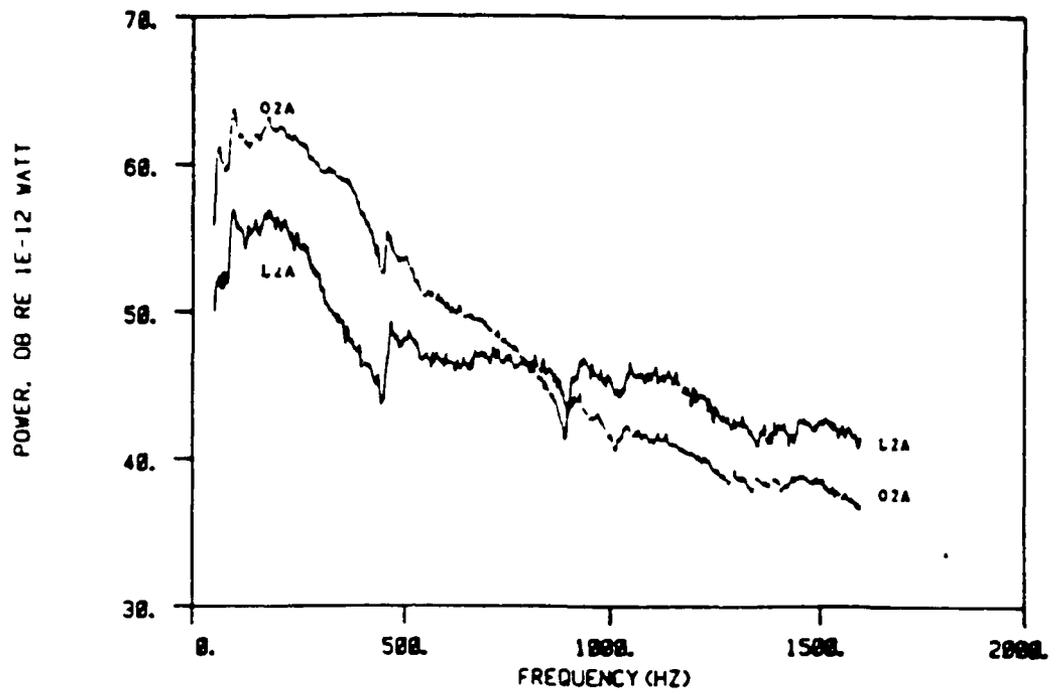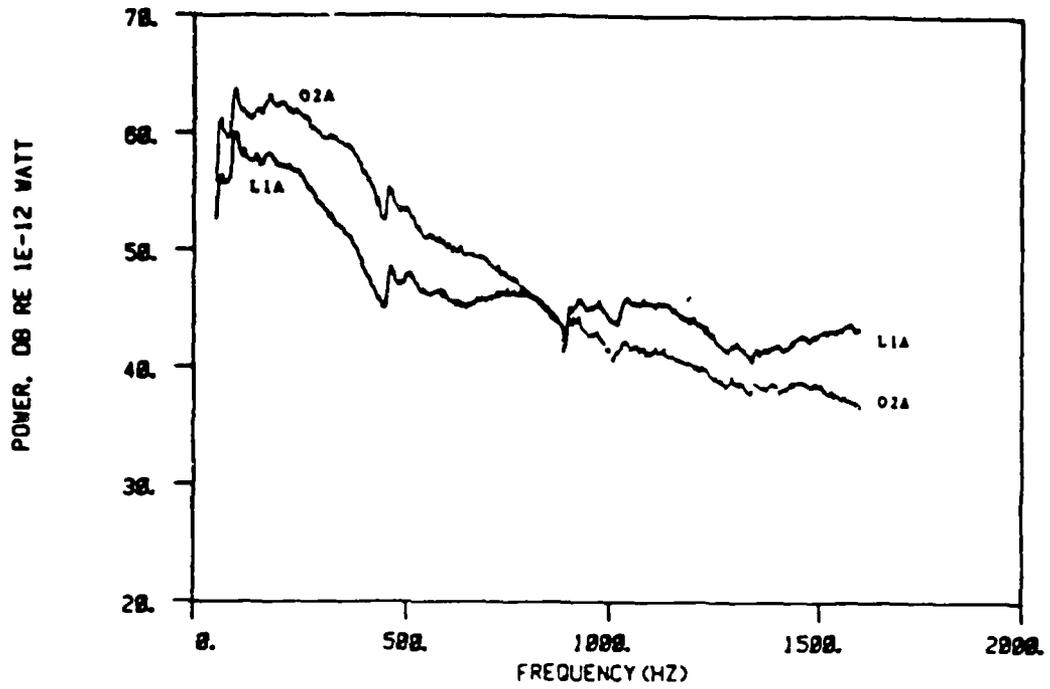
Figure 47: Effect of louvering on sound power spectral level, L-1A versus O-2A
at $U = 50\ m/s$

Thus one can conclude that effective louvering does reduce the total radiated power by reducing single mode resonance and by inter fering with the lower frequency, longitudinal eddy correlation. This results in effectively broadening the power spectrum.

5.9.4 Louver geometry effect on sound power

As with the straight walled louvers, the multiple circular aperture louver was quieter than the multiple rectangular aperture louver by 1.4 to 3.6 dB in total radiated power. As shown in Figures 39 and 40, louver L-2A had approximately the same spectral shape as louver L-1A but with considerably less power in the low frequency bands. Again this reduction can be attributed to the additional interference of the lateral correlation due to the reduced dimension in the aperture's height. To test this conclusion, one can calculate the frequency where the lateral correlation length, ℓ, equals the aperture diameter, d for louver L-2A and at freestream velocity of 50 m/s. From Figure 8, at $B(Kr_3) = 0.4$, the value of $Kr3$ equals 1.2. Setting Kr_3 equal to 0.01 m (27/64″) and $U = 50$ m/s gives a limiting frequency of 450 Hz. Thus one would predict diminishing reductions in sound power for frequencies above 450 Hz. Reference to Figure 49 shows that, indeed, at frequencies above 450 Hz the effect of lateral correlation interference on reducing sound power is diminishing.

5.10 Describing the Velocity Field Surrounding the Samples

In Section 3, the radiated sound power was shown to be directly related to the normal component of the turbulent intensity. Several measurements of the turbulent intensity spectrum were taken as described in Section 4.4. The assumption was made that the turbulent intensity in the streamwise direction was six times that in the normal direction, based upon measurements of corresponding r.m.s. velocity component values in the most active region of turbulent boundary layer near the wall, Klebanoff [18]. Thus 8 dB was subtracted from the measured intensity spectral levels to give only the normal component of the turbulent fluctuations. The following observations are made:

- the turbulent intensity measured 2 tenths of an inch into the boundary layer was relatively unaffected by the probe location in the transverse direction and the various orifice geometries. Figure 50 is the measured normal component of the turbulent intensity for louver L-1, with the probe at the center of the upstream aperture. These spectral levels were used in the following section to collapse the sound power spectra.
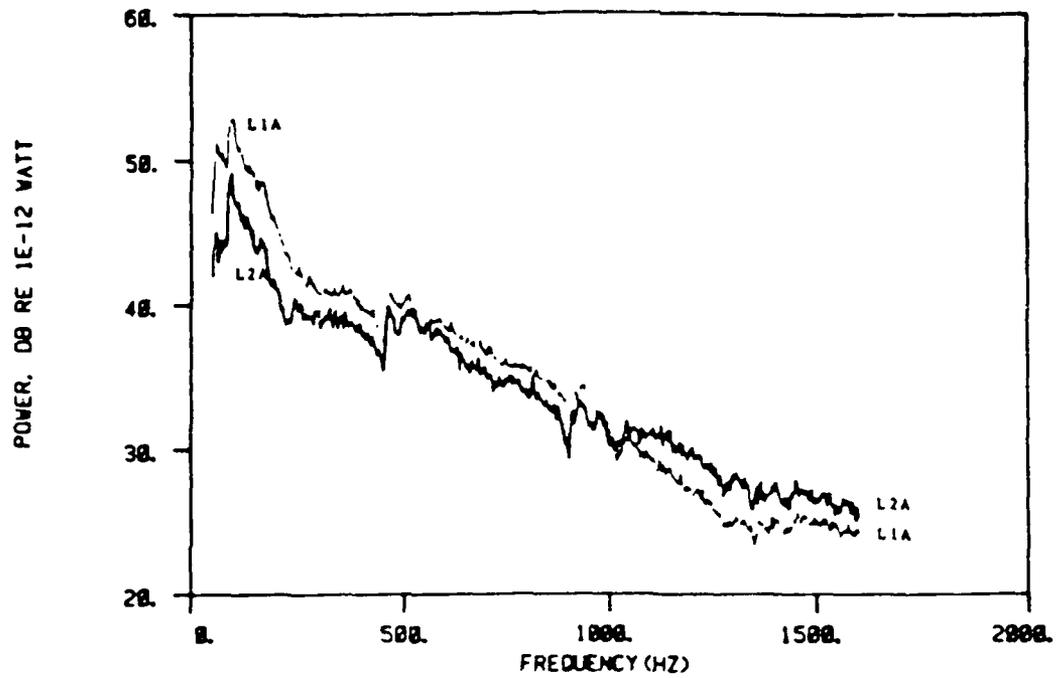
73

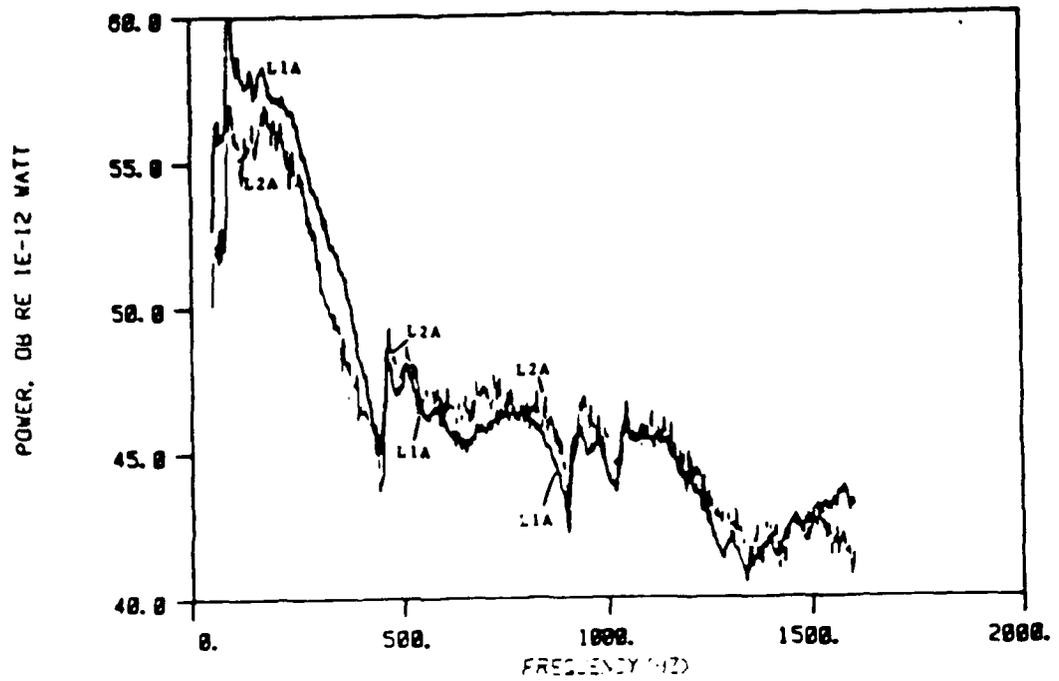Figure 48: Louver geometry effect on sound power spectral level, L-1A versus L-2A at $U = 30 \, m/s$.

Figure 49: Louver geometry effect on sound power spectral level, L-1A versus L-2A at $U = 50\ m/s$.
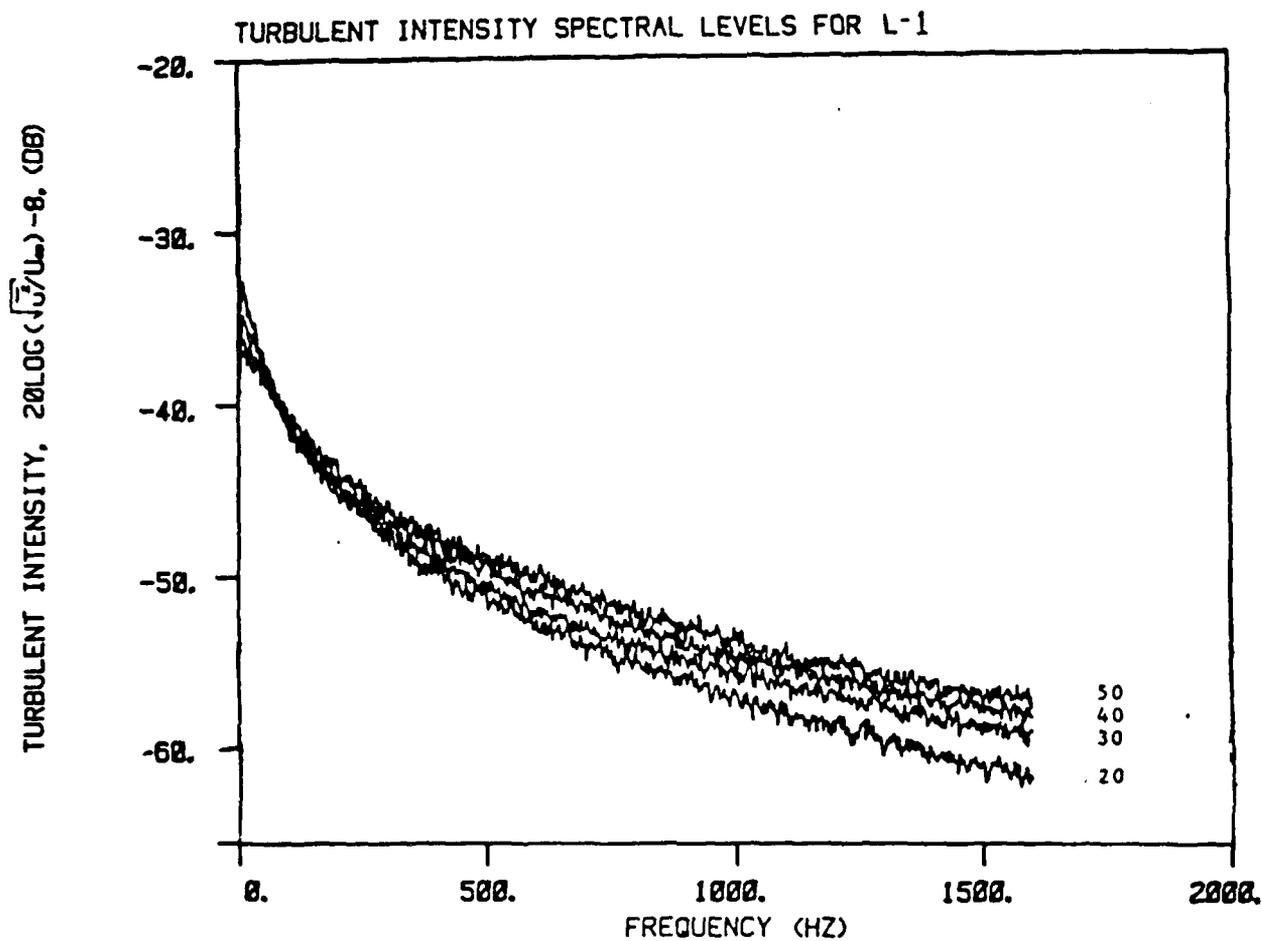
75

Figure 50: Turbulent intensity spectral levels for louver L-1 versus freestream velocity.

- there were significant reductions in turbulent intensity (approximately 3 dB) between louvers L-1 and L-1A when measured at the leading edge of the leading aperture. This reduction in intensity supports the measured reduction in total sound power and also supports the conclusions that the sound power is related to the driving aerodynamic field.

Despite a fairly rigorous attempt to maintain the block-house air tight, a finite and measurable pressure differential existed between the blockhouse and the duct static pressure. This pressure differential resulted in a small amplitude, mean flow entering the orifice/louver from the closed acoustic space. The magnitude of this transverse mean flow was greatest in the louver samples and measured on average, fourteen percent of the freestream velocity. The exact contribution of this mean flow to the radiated sound power in not known but it is estimated to be of minimal impact since the turbulent intensity of the entering flow measured several orders of magnitude less than the normal component of the freestream turbulence.

5.11 Verifying the Scaling Laws

In Section 3, an equivalent source model was developed for rectangular shaped aperture orifices and louvers. To ascertain the validity of this model, the sound power spectra for orifices O-2, O-3 and the louver L-1 were collapsed by normalizing the spectral levels by the magnitude of the equivalent source model. The resulting collapsed spectra are shown in Figures 51, 52 and 53. It is evident by the collapse that the equivalent source model adequately describes the controlling parameters for orifice and louver flow noise. The prediction of the actual magnitude of the sound power is fairly accurate for the samples with the smaller apertures but is too high by about 7 dB for the larger aperture openings (O-1 and O-2). The probable reasons for this are (1) overestimating the effective aperture width, b, and (2) the estimation for the lateral correlation lengths. As mentioned in Section 3, for orifice O-2, the longitudinal correlation amplitude function, $A(K(\epsilon_1))$ does attenuate to a value of approximately 0.6 for the slower speeds indicating that some eddy decay occurred in the aperture. For this case, one could assume a smaller transverse length, b', over which the eddy decay was minimal and use this length scale for evaluating the source strength. Defining b' at the point where the magnitude of the amplitude function equaled 0.95 results in an effective aperture length of 0.5 inches versus the actual dimension of $b = 1.67$ inches (for orifice O-2 at $U = 20 \ m/s$ and $f = 250$ Hz). This
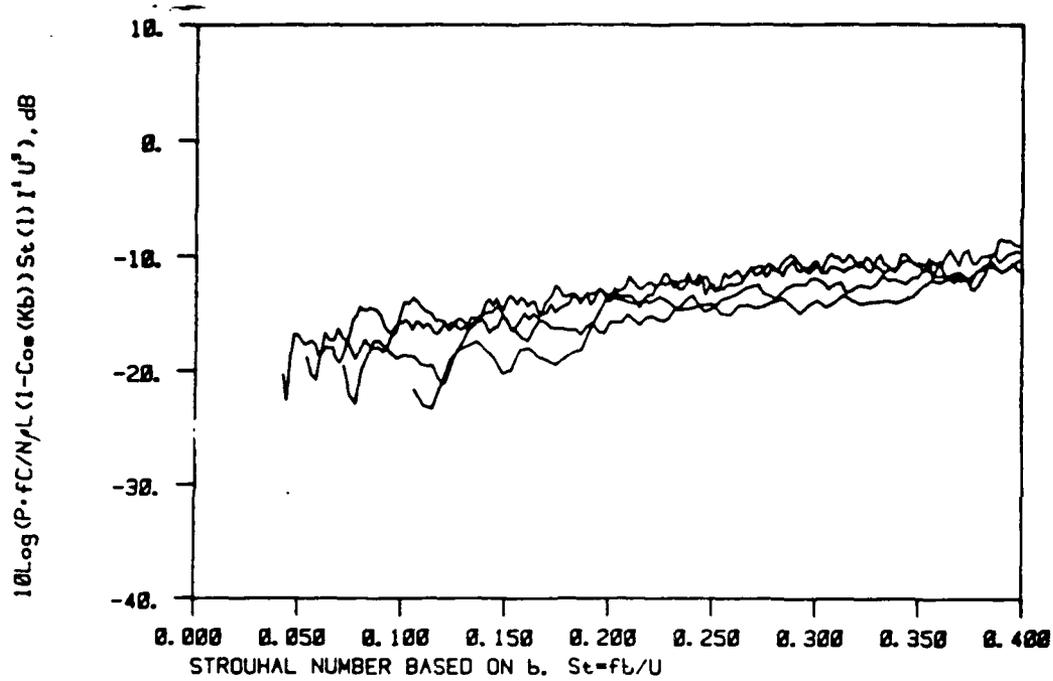
77

Figure 51: Scaling law verification for orifice O-2

results in a reduction of 4.2 dB in the predicted spectral level and could account for some of the error in predicting the larger aperture radiated sound power.
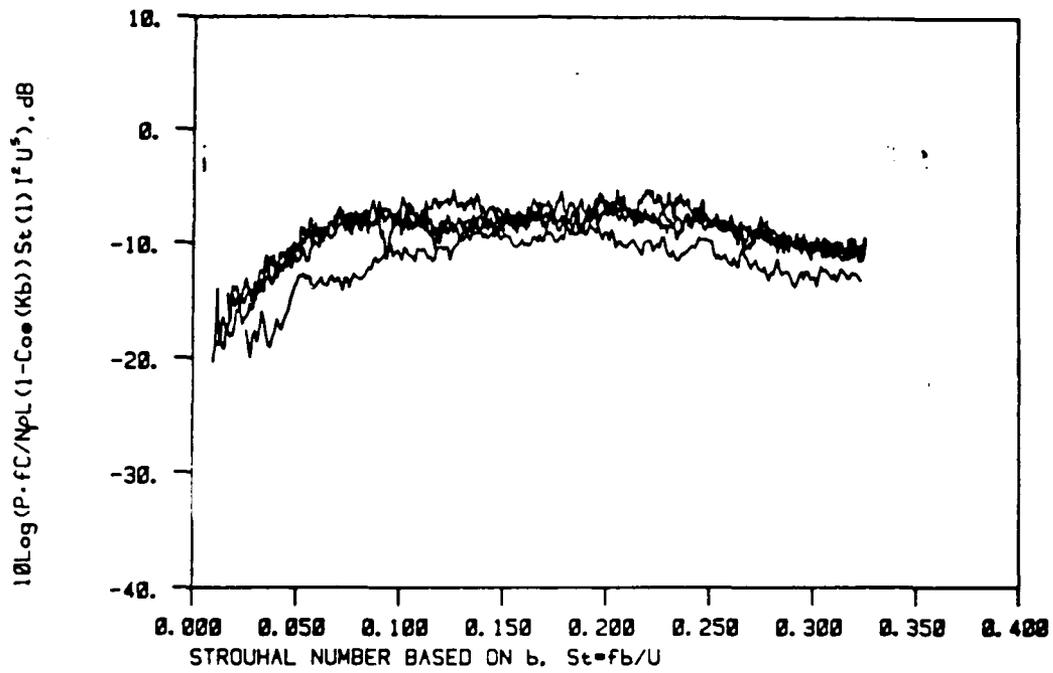
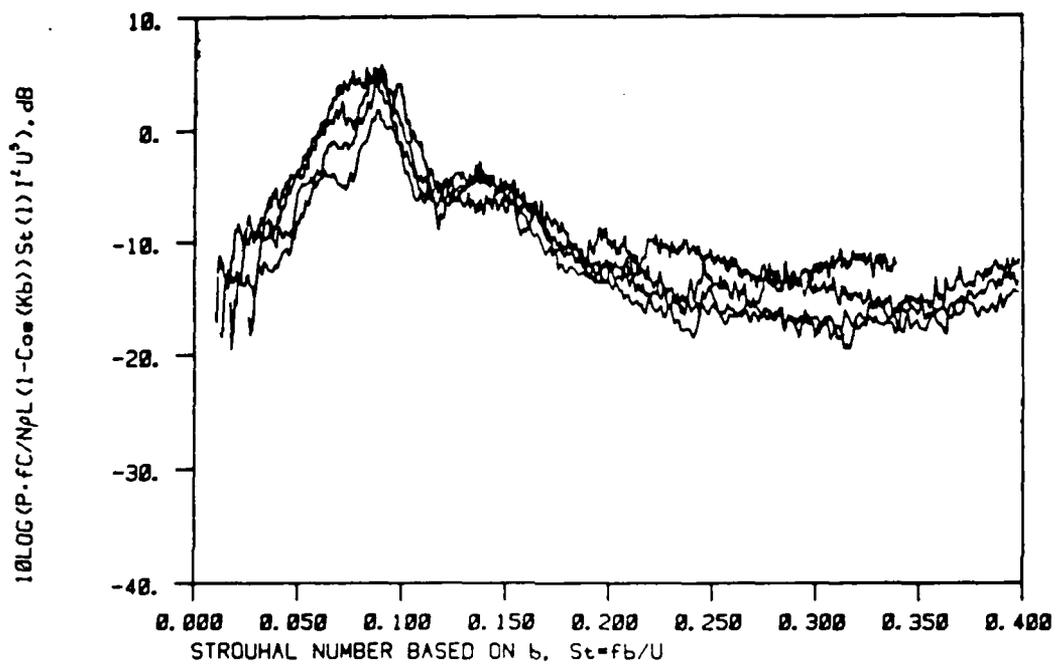Figure 52: Scaling law verification for orifice O-3

Figure 53: Scaling law verification for louver L-1

80

6. CONCLUSIONS

The acoustic source created by turbulent flow over orifices and louvers was investigated by measuring the radiated sound intensity, utilizing an intensity probe, at various wind speeds in a semi-anechoic wind tunnel. From the intensity spectra, the radiated power and the directivity of the source was determined. The goal of this research was to describe the source and identify the controlling parameters which affect its spectral shape, radiated power and directivity. The orifice and louvers investigated have geometries similar to those used in industry in both air and water environments. The effects of various leading/trailing edge geometries were also investigated.

The source of noise has been modelled on the basis of theoretical analyses by Ffowcs Williams, Nelson and Corcos. The equivalent source of noise was modelled as two equal but opposite monopole sources located in the upper and lower aperture of each orifice. The strength of each source is determined by the mass flow driven through the apertures by the normal component of the turbulent fluctuations. The resulting radiated sound field, both into a closed acoustic space and radiating away from the orifice, is dependent on the acoustical properties of the louver.

To ascertain the validity of the source model, two orifice and one louver power spectra were collapsed by normalizing the spectral levels by the magnitude of the equivalent source model. It is evident by the collapse that the equivalent source model adequately describes the controlling parameters for orifice and louver flow noise. The controlling parameters for the geometries tested were:

1. Strouhal number based on the lateral correlation length, ℓ, and aperture transverse dimension, b

2. the normal component of the Turbulent Intensity,

3. the fifth power of the freestream velocity and

4. the shape factor $(1 - \cos(Kb))$ where K is the convective wavenumber, $K = \omega/Uc$, and Uc is the eddy convection velocity.

As a result of this research, several important conclusions are made:

- sound intensity measurements, using an intensity probe, can successfully describe an acoustic source, even though measurements are taken within the source's near field.

81

- the errors associated with measuring intensity, using an intensity probe, can be as small as the inherent statistical deviation of the random fluctuations.

- the equivalent source model developed to describe the behavior of orifice and louver flow noise successfully describes the controlling parameters and provides valuable insight for predicting the actual magnitudes of the radiated sound spectrum.

- the 1/3 octave band containing the most acoustic power from orifice and louver flow noise can be predicted from the non-dimensional Strouhal number based on the aperture's transverse dimension and the non-dimensional length scale,δ/b where δ is the turbulent boundary layer thickness.

- for aerodynamic flows, the orifice/louver source provides both the dominant amount of total sound power and the spectral character of the radiated noise. Contributions due to structural radiation from the ducting and ducting "open window" effects are not significant.

- the effect of louvering, simply by dividing the total open area into more numerous, smaller areas does not by itself reduce the total radiated flow noise and will most probably result in increased radiated sound power in the higher frequency bands.

- the effect of reducing the aperture throat thickness is to broaden the spectral shape of the radiated power spectrum while maintaining approximately the same total radiated sound power.

- the effect of reducing the aperture's transverse dimension can be adequately described by the controlling shape factor in the equivalent source model, $(1 - \cos(Kb))$.

- directivity measurements show a nearly omni-directional source in the on-axis planes with off-axis power levels reduced by 2-3 dB.

- taken together, the effect of louvering and angling the leading and trailing edges resulted in reductions to sound power of 3.4 -7.5 dB compared to the equivalent area, single aperture, angled orifice.

- the measured reductions in sound power due to effective louvering can be explained by (1) reductions in the normal component of the turbulent intensity due to the eddies impacting a blunt trailing edge and (2) destructive interference with the eddy longitudinal and lateral correlations.

82

- the louvers with numerous circular apertures and angled edges radiated the least acoustic power with a very broad, flat power spectrum.

REFERENCES

1. Powell, A., "On Edge Tones and Associated Phenomena," *Acustica*, Vol. 3, pp. 233-243, 1953.

2. Dunham, W. H., "Flow-Induced Cavity Resonance in Viscous Compressible and Incompressible Fluids", Rept. ARC-73, Office of Naval Research, 4th Symposium of Naval Hydrodynamics, Vol. 3, Washington, D.C., 1962.

3. Rossiter, J. E., "Wind Tunnel Experiments on the Flow over Rectangular Cavities at Subsonic and Transonic Speeds", Royal Aircraft Establishment, Tech. Report No. 64037, Oct. 1964.

4. East, L. F., "Aerodynamically Induced Resonance in Rectangular Cavities," *JSV*, 3(3), pp. 277-287, 1966.

5. 5. DeMetz, F. C. and Farabee, T. M., "Water-Flow Induced Cavity Resonances,", David Taylor Naval Ship Research and Development Center Report, SAD-132E-1942, February, 1976.

6. Grade, S., K. G. Ginn, O. Roth and M. Broch, "Sound power determination in high reactive environments using sound intensity measurements", Bruel and Kjaer application notes.

7. Bruel & Kjaer, "Sound intensity analyzing system type 3360", Jan. 1983.

8. Ffowcs Williams, J. E., "The acoustics of turbulence near sound absorbent liners", *Journal of Fluid Mechanics* 51, pp. 737-749, 1972.

9. Nelson, P. A., "Noise generated by flow over perforated surfaces", *Journal of Sound and Vibration* (1982) 83(1), 11-26.

10. Leppington, F. G. and H. Levine, "Reflection and transmission at a plane screen with periodically arranged circular performation", *Journal of Fluid Mechanics* 61, 1973, 109-127.

11. Nelson, P. A., "Aerodynamic sound production in low speed flow ducts", PhD thesis, University of Southampton, 1979.

12. Corcos, G.M., "Resolution of pressure in turbulence", *J. Acoust. Soc. Am.*, 35, 1963, 192-199.

REFERENCES (Continued)

13. Hanson, C.E., "The design and construction of a low-noise low turbulence wind tunnel", MIT Engineering Projects Laboratory Report # 79611-1, January 1969.

14. Shapiro, P. J., "The influence of sound upon boundary layer transition", MIT Acoustic and Vibration Lab Report, 83458-83560 -1, September, 1977.

15. Spinka, N.S., "Acoustic levels in a low turbulence wind tunnel", MIT, MSc. Thesis, February, 1974.

16. Bolt, Beranek and Newman, "A review of flow noise research related to the sonar self noise problem", Department of the Navy, Report No. 4110366, March, 1966.

17. Townsend, A. A., "The Structure of Turbulent Shear Flow", New York: Cambridge University Press, 1976.

18. Klebanoff, P. S., NACA Tech. Notes, 3178, 1954 reproduced in Hinzem J. 6, "Turbulence", McGraw-Hill, 1959, p. 488.

APPENDIX 1:
MATCHED ASYMPTOTIC EXPANSION SOLUTION TO A RADIATING ORIFICE IN AN INFINITE RIGID WALL

The two dimensional problem to be solved is the far field radiated pressure at x_k, created by a driving aerodynamic field at y_k, within a finite size aperture in an infinite, rigid wall. Using the principle of reciprocity, the above field can be determined by first solving for the sound field at y_k created by a distant monopole at x_k. Then, the desired solution is obtained by simply replacing the position vectors of the far field monopole and the aperture source. The solution to this problem will be analyzed using the principles of Matched Asymptotic Expansions (MAE).

The coordinate system used in the analysis is shown below.
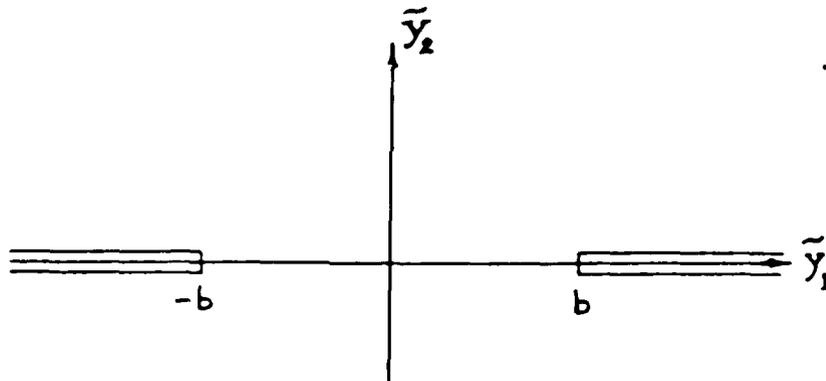
with boundary conditions, $\partial \tilde{p}/\partial \tilde{y}_2 = 0$ for $|\tilde{y}_1| \geq b$ and $\tilde{y}_2 = 0$.

The governing equations for a plane wave of single frequency, ω, at normal incidence are:

$$\tilde{\nabla}^2 \tilde{p} + k^2 \tilde{p} = 0 \qquad (A1.1)$$

$$\tilde{p} = A e^{i(k\tilde{y}_2 - \omega t)} \qquad (A1.2)$$

where k is the acoustic wavenumber, $k = \omega/c_0$. Also define the non-dimensional terms, $\tau = \omega t, y_1 = k\bar{y}_1, y_2 = k\bar{y}_2, p = \bar{p}/A$ and $\epsilon = kb$ for the parameters in the outer problem.

Substituting the above outer parameters into equations A1.1 and A1.2 gives the governing equations and boundary condition for the outer problem

$$\nabla^2 p + p = 0 \qquad\qquad (A1.3)$$

$$p = e^{i(y_2 - \tau)} \qquad\qquad (A1.4)$$

To lowest order, $\epsilon \to 0$, and the orifice closes. Thus the outer problem becomes

$$p \sim \delta_1 p_1 + \delta_2 p_2 + \cdots \text{ as } \epsilon \to 0 \qquad\qquad (A1.5)$$

with $\delta_1 = 1$. From the boundary condition, we can determine p_1 to be

$$p_1 = p_i + p_r = e^{iy_2} + e^{-iy_2}, \quad y_2 < 0 \qquad\qquad (A1.6)$$

suppressing the $e^{-i\tau}$ factor, where p_i, p_r are the incidence and reflected waves, respectively. Note that the boundary condition is satisfied

$$\frac{\partial p_1}{\partial y_2} = \left(e^{iy_2} - e^{-iy_2}\right) = 0 \quad \text{for } y_2 = 0. \qquad\qquad (A1.7)$$

Choose also the condition that $p_1 \equiv 0$ for $y_2 > 0$. To open the orifice, choose the inner variables $\bar{y}_1 = y_1/\epsilon$ and $\bar{y}_2 = y_2/\epsilon$.

In inner variables,

$$\begin{aligned}
p &= exp\big(i(\epsilon\bar{y}_2 - \bar{\tau})\big) + exp\big[-i(\epsilon\bar{y}_2 - \bar{\tau})\big] \\
&= exp(-i\bar{\tau})\{exp(\epsilon\bar{y}_2) + exp(-\epsilon\bar{y}_2)\} \\
&\sim exp(-i\bar{\tau})\Big\{1 + \epsilon\bar{y}_2 - \frac{\epsilon^2\bar{y}_2^2}{2} - \cdots + 1 - \epsilon\bar{y}_2 - \frac{\epsilon^2\bar{y}_2^2}{2} + \cdots\Big\} \\
&= 2e^{-i\bar{\tau}}\Big\{1 - \frac{\epsilon^2\bar{y}_2^2}{2} + \mathcal{O}(\epsilon^4)\Big\} \quad \text{as } \epsilon \to 0, \bar{y}_2 \text{ fixed } (y_2 \to 0). \qquad (A1.8)
\end{aligned}$$

The governing equation with the inner parameters substituted into equations A1.3 becomes

$$\bar{\nabla}^2\bar{p} + \epsilon^2\bar{p} = 0 \qquad\qquad (A1.9)$$

with boundary conditions $\partial\bar{p}/\partial\bar{y}_2 = 0$ for $\bar{y}_2 = 0$ and $|\bar{y}_1| \geq 1$. Let $\bar{p}$ be defined by

$$\bar{p} \sim \Delta_0(\epsilon)\bar{p}_1 + \Delta_1(\epsilon)\bar{p}_2 + \cdots \qquad\qquad (A1.10)$$

for the inner expansion. The resulting inner problem coordinate system is
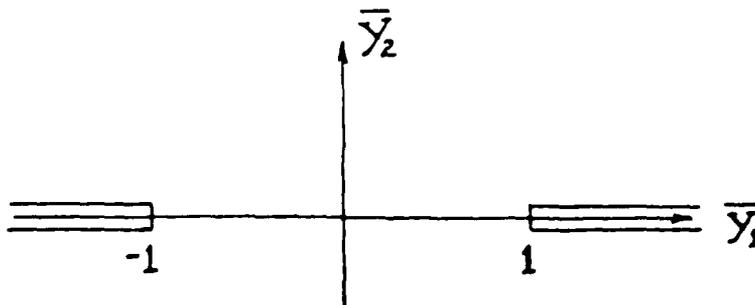
Since $\bar{\nabla}^2\bar{p}_1 = 0$, solve the inner problem by conformal mapping, $\bar{p}_1 = ARe(w)$. Using a solution of the form, $i\bar{z} = \cosh w$, (suppressing the $e^{-i\bar{\tau}}$ factor) we can determine

$$w \sim \ell n 2\bar{z} + i\pi/2 + \frac{1}{2\cdot 2\bar{z}^2} - \frac{1\cdot 3}{2\cdot 2\cdot 4\bar{z}^4} + \cdots \text{as } |\bar{z}| \to \infty \qquad (A1.11)$$

where

$$\bar{z} = \bar{r}e^{i\theta}.$$

Since

$$\bar{z} = z/\epsilon,$$

$$w \sim \ell n2z - \ell n\epsilon + i\pi/2 + O(\epsilon^2) \quad \text{for } \epsilon \to 0, \ z \ \text{fixed}(\bar{z} \to \infty) \qquad (A1.12)$$

Therefore, utilizing equation A.11, we can determine $\Delta_0(\epsilon)\bar{p}_1$ to be

$$\Delta_0(\epsilon)\bar{p}_1 \sim A\Delta_0\{\ell n2\bar{r} - \ell n\epsilon + i\pi/2 + O(\epsilon^2)\}. \qquad (A1.13)$$

Now matching the leading terms in the outer and inner solutions, equations A1.8 and A1.13, leads to $\Delta_0 = +1/\ell n\epsilon$ and $A = -2$. Then $\delta_2(\epsilon) = 1/\ell n\epsilon$ in the outer expansion. p_2 satisfies the Helmholtz equation with $k = 1$ and must behave like ℓnr for $r \to 0, \epsilon \to 0$ and $\bar{r}$ fixed. Clearly

$$p_2 = CH_0^{(1)}(r) \qquad (A1.14)$$

satisfies this requirement and also satisfies the rigid wall condition. As $r \to 0$,

$$H_0^{(1)}(r) \sim \frac{2i}{\pi}\ell nr + 1 + \frac{2i}{\pi}(\gamma - \ell n2) + \cdots$$

where γ is defined as Euler's constant. Thus to match with the inner solution, $A = -2 = C \cdot 2i/\pi$, C must be equal to $i\pi$. Therefore the final outer expansion becomes

89

$$p \sim e^{-i\tau} \left\{ e^{\nu_2} + e^{-\nu_2} + \frac{i\pi H_0^{(1)}(\tau)}{\ell n \epsilon} + \cdots \right\} \qquad (A1.15)$$

where the first term in brackets is the incident wave, the second term is the reflected wave and the lowest order orifice effect is the last term which describes a monopole type radiation. Substituting for the non-dimensional terms and applying the principle of reciprocity, one obtains the radiated sound from a 2 dimensional, single slot, line source

$$\tilde{p} \sim A \left\{ e^{k\tilde{z}_2} + e^{-k\tilde{z}_2} + \frac{i\pi H_0^{(1)}(\tilde{r})}{\ell n k b} \right\} e^{-i\omega t} \qquad (A1.16)$$

As $\tilde{r} \to \infty$, $H_0^{(1)}(\tilde{r}) \to \sqrt{2/\pi \tilde{r}} e^{i(\tilde{r} - \pi/4)}$ so the far field radiated sound for the 2D, single slot, line source becomes

$$\tilde{P}_{r \to \infty} \sim A \left\{ e^{k\tilde{z}_2} + e^{-k\tilde{z}_2} + i\pi \sqrt{2/\pi \tilde{r}} e^{i(\tilde{r} - \tilde{r}/4)} \right\} e^{-i\omega t}. \qquad (A1.17)$$

Equation A1.17 provides the result that the far field radiated pressure for a 2D, single slot source to lowest order is composed of:

1. the incident and rigid wall reflection

2. 2D line source having a 1/r dependence (cylindrical spreading).

Thus one can infer that it is plausible for the 3 dimensional, single orifice source to have a reflection coefficient, $|R|^2 \approx 1$ for values of $b/\lambda \ll 1$.

90

APPENDIX 2:
MEASURING TURBULENT INTENSITY

In this appendix, the transfer function to relate the mean and fluctuating component of the hot wire anemometer output voltage to the mean and fluctuating component of the particle velocity is developed.

The basic relationship between output voltage, E, and particle velocity, U, is defined by King's Law

$$E = A + BU^n \qquad (A2.1)$$

Now define the instantaneous voltage and particle velocity by

$$E = E_0 + e' \quad and \mid e' \mid \ll \mid E_0 \mid \qquad (A2.2)$$

$$U = U_0 + u' \quad and \mid u' \mid \ll \mid U_0 \mid \qquad (A2.3)$$

where E_0 is the mean of E, U_0 is the mean of U, e' and u' are the fluctuating components whose expectations are zero. Substituting equations A2.2 and A2.3 into equation A2.1, expanding and dropping the higher order terms of u' and e' gives

$$E_0^2 + 2E_0 e' = A + BU_0^n(1 + \lfloor nu'/U_0 \rfloor) \qquad (A2.4)$$

Taking the expectation of equation A2.4 gives

$$E_0^2 = A + BU_0^n. \qquad (A2.5)$$

91

Subtracting equation A2.5 from equation A2.4 gives the desired relationship between the fluctuating components of the anemometer output voltage, e', and the particle velocity, u',

$$u' = ([2E_0 U_0^{1-n}]/Bn)e'. \qquad (A2.6)$$

Thus, defining the term in parentheses as H, the resulting relationship between the spectral densities of the fluctuating velocity, $S_u(f)$, and the output voltage, $S_E(f)$, is

$$S_u(f) = |H|^2 S_E(f). \qquad (A2.7)$$

APPENDIX 3:
MATHEMATICAL STEPS IN DETERMINING
$S_Q(y_k, \omega)$

From equation 3.7, the cross spectral density is assumed to be of the form

$$S_{vv}(\epsilon_k, \omega) = S_v(y_k, \omega) A(K\epsilon_1) B(K\epsilon_3) \cdot exp(iK\epsilon_1). \qquad (A3.1)$$

As described in Section 3.2, the longitudinal correlation amplitude function, $A(K\epsilon_1)$, is identically equal to one for all samples except O-1 and O-2 at the lower freestream velocities, where at a minimum it equals 0.6. So assuming no decay in the eddy structure in the y_1 direction (i.e., $A(K\epsilon_1)$ equals one) and $S_v(y_k, \omega)$ to be uniform over the aperture surface, the source strength spectral density becomes

$$S_Q(y_K, \omega), = \rho^2 \omega^2 S_v(y_k, \omega) \int_\infty \int_\infty B(K\epsilon_3) exp(iK\epsilon_1) \theta(\epsilon_k) dA(\epsilon k) \qquad (A3.2)$$

where ϵ_1, ϵ_3 are the position coordinates as shown below.
Substituting for $\theta(\epsilon_k)$ we have

$$S_Q(y_k, \omega) = \rho^2 \omega^2 S_v(y_k, \omega) \int_\infty \int_\infty B(K\epsilon_3) e^{ik\epsilon_1} (L - \mid \epsilon_3 \mid)(b - \mid \epsilon_1 \mid) \cdot dA(\epsilon_k).$$
$$(A.3.2a)$$

Since the lateral correlation ℓ is typically one-tenth or less the length of the aperture, the integral in the ϵ_3 direction can be evaluated, independent of the actual limits of the integrand, as

$$\int_\infty B(K\epsilon_3)(L - \mid \epsilon_3 \mid) d\epsilon_3 = L\ell - O(\ell^2) \qquad (A3.3)$$

where

93

$$\int_{\infty} B(K\epsilon_3)d\epsilon_3 = \ell. \qquad (A3.3a)$$

Evaluating the integral over the ϵ_1 directions gives:

$$\int_{\infty} e^{ik\epsilon_1}(b- \mid \epsilon_1 \mid)d\epsilon_1 = \frac{2}{K^2}(1 - \cos(Kb)). \qquad (A3.4)$$

Therefore the final result, neglecting the ℓ^2 term is:

$$S_Q(y_k,\omega) = \rho^2\omega^2 S_v(y_k,\omega)L\ell(\frac{2}{K^2})(1 - \cos(Kb)). \qquad (A3.5)$$

The remaining term needed to fully describe the magnitude of the source strength spectral density is ℓ. The lateral correlation length, ℓ, is determined at the point where the amplitude function, $B(K\epsilon_3)$ equals 0.4 and the frequency equals the center frequency, f_C, as defined in Section 5.3.